



UNIVERSIDAD DE CUENCA

Facultad de Ingeniería

Maestría en Hidrología con mención en Ecohidrología

**FACTORS CONTROLLING THE STABLE ISOTOPIC COMPOSITION
OF PRECIPITATION IN THE TROPICAL ALPINE HIGHLANDS OF
SOUTH ECUADOR**

Trabajo de titulación previo a la
obtención del título de Máster
en Hidrología con mención en
Ecohidrología

Autor:

Ing. Darío Xavier Zhiña Villa

CI: 010504448-1

Correo electrónico: xavidx2008@hotmail.com

Director:

Ing. Giovanny Mauricio Mosquera Rojas PhD.

CI: 010445091-1

CUENCA-ECUADOR

08-septiembre-2021

**Resumen:**

La composición isotópica de la precipitación proporciona información valiosa sobre los factores que influyen en la precipitación local en las zonas montañosas. Dicha información puede ayudar a mejorar la gestión de los recursos hídricos a la luz de los cambios en el clima global. Los isótopos estables en el agua (WSI) proporcionan información sobre los factores que influyen en la precipitación, como el reciclaje de humedad regional y/o la re-evaporación local que afecta la precipitación en un sitio de estudio determinado. Además, el uso de modelos de transporte Lagrangiano puede ayudar a identificar fuentes de humedad que contribuyen a la precipitación local y proporcionar información sobre factores climatológicos regionales que influyen en su composición isotópica. En los Andes tropicales, la comprensión de la precipitación local y la aplicación de WSI y modelos Lagrangianos pueden ayudar a llenar esta brecha de conocimiento que sigue siendo limitada debido principalmente a la falta de datos isotópicos recopilados a alta resolución temporal. (sub-diario). Por lo tanto, este estudio tiene como objetivo investigar los factores que influyen en la composición isotópica de la precipitación en las tierras altas alpinas tropicales (Páramo) del sur de Ecuador utilizando un conjunto de datos de WSI recopilados a alta resolución temporal durante el período octubre de 2017 a octubre de 2018. Los resultados mostraron que existen cuatro trayectorias principales que siguen las masas de aire (llanuras del Orinoco, cuenca del Amazonas, Macizo de Mato Grosso y Océano Pacífico) antes de llegar al sitio de estudio. También se encontró que los factores regionales son los que controlan en gran medida la composición isotópica de la precipitación WSI, aunque también se encontró que la actividad convectiva en el sitio de estudio es un controlador de la misma. Los factores encontrados para $\delta^{18}\text{O}$ resultaron explicar gran parte de la varianza de la composición isotópica, sin embargo, para el D-excess los factores no explicaron altos porcentajes de varianza. Los resultados obtenidos en este estudio pueden ayudar a mejorar los modelos climáticos utilizando WSI o incluso ayudar a las reconstrucciones paleoclimáticas en los Andes tropicales.

Palabras claves: Isótopos estables. Precipitación. Páramo $\delta^{18}\text{O}$ y D-excess.

**Abstract:**

The isotopic composition of precipitation provides valuable information about the factors influencing local precipitation in mountainous areas. This information can help improve the management of water resources in light of changes in global climate. Water Stable Isotopes (WSI) provide information on factors influencing precipitation, such as regional moisture recycling and/or local re-evaporation that affects precipitation at a given study site. The use of Lagrangian transport models can help identify sources of moisture that contribute to local precipitation and provide information on regional climatological factors that might influence the isotopic composition of local precipitation. In the tropical Andes, the understanding of local precipitation and the application of WSI and Lagrangian models that can help fill this knowledge gap remains limited mainly due to the lack of precipitation isotope data sets collected at high temporal frequency (sub-daily to storm-based sampling). Therefore, this study aims to investigate the factors influencing the isotopic composition of precipitation in the tropical alpine highlands (Páramo) of southern Ecuador using a set of WSI data collected at high-temporal frequency during the period October 2017 to October 2018. Results show that there are four main trajectories that the air masses follow (Orinoco plains, Amazon basin, Mato Grosso Massif, and Pacific Ocean) before reaching the study site. Similarly, it was found that regional factors are what largely control the WSI composition of precipitation, although it was also found that convective activity at the study site is a controller of the isotopic composition. The factors found for $\delta^{18}\text{O}$ signal turned out to explain a large part of the isotopic composition variance, however for D-excess the factors did not explain a high percentage of variance. The results obtained in this study can help to improve climate models using WSI or even help paleoclimate reconstructions in the tropical Andes.

Keywords: Stable isotopes. Precipitation. Páramo. $\delta^{18}\text{O}$ y D-excess.



ÍNDICE DEL TRABAJO

CONTENIDO

1. INTRODUCTION.....	10
2. MATERIALS AND METHODS.....	13
2.1 Study site.....	13
2.2 Meteorological data collection.....	14
2.3. Isotopic data collection and laboratory analysis	15
2.4. Origin and trajectories of water vapor masses	17
2.5. LMWL and D-excess analysis	18
2.6. Analysis of factors controlling the isotopic composition of precipitation	19
3. RESULTS	21
3.1 Description of meteorological conditions.....	21
3.2 Isotopic composition	21
3.3 Origin and trajectories of water vapor masses	23
3.4 Factors controlling the isotopic composition of precipitation	26
4. DISCUSSION.....	30
4.1 Isotopic composition	30
4.2 Origin and trajectories of water vapor masses	31
4.3 Factors controlling the isotopic composition of precipitation	31
5. CONCLUSIONS.....	35
6. REFERENCES	36
7. SUPPLEMENTARY MATERIAL.....	45



ÍNDICE DE FIGURAS

Figure 1. The Zhurucaay Ecohydrological Observatory (ZEO) situated in south Ecuador..	14
Figure 2. <i>Regions considered as sources of moisture through which the air masses travel before reaching the study area.</i>	18
Figure 3. Time series of meteorological in situ variables and time series of isotopic composition.	22
Figure 4. $\delta^2\text{H}$ - $\delta^{18}\text{O}$ diagram constructed with the precipitation samples collected during October 2017 – November 2018..	23
Figure 5. The trajectories of the air masses corresponding to the trajectories of: a) Orinoco plains, b) Pacific coast and c) Mato Grosso Massif and d-f) Amazon basin..	24
Figure 6. X-Y graph of the observed and simulated isotopic composition of $\delta^{18}\text{O}$ with the Multiple Linear Regression (MLR) for their respective trajectories.....	28

ÍNDICE DE TABLAS

Table 1. Results of performing the Multiple Linear Regression (MLR) for $\delta^{18}\text{O}$ after using the stepwise criterion.	29
---	----



Cláusula de licencia y autorización para publicación en el Repositorio Institucional

Yo, Darío Xavier Zhiña Villa en calidad de autor y titular de los derechos morales y patrimoniales del trabajo de titulación "Factors controlling the stable isotopic composition of precipitation in the tropical alpine highlands of south Ecuador", de conformidad con el Art. 114 del CÓDIGO ORGÁNICO DE LA ECONOMÍA SOCIAL DE LOS CONOCIMIENTOS, CREATIVIDAD E INNOVACIÓN reconozco a favor de la Universidad de Cuenca una licencia gratuita, intransferible y no exclusiva para el uso no comercial de la obra, con fines estrictamente académicos.

Asimismo, autorizo a la Universidad de Cuenca para que realice la publicación de este trabajo de titulación en el repositorio institucional, de conformidad a lo dispuesto en el Art. 144 de la Ley Orgánica de Educación Superior.

Cuenca, 8 de septiembre de 2021

Darío Xavier Zhiña Villa

010504448-1



Cláusula de Propiedad Intelectual

Yo, Darío Xavier Zhiña Villa, autor del trabajo de titulación "Factors controlling the stable isotopic composition of precipitation in the tropical alpine highlands of south Ecuador", certifico que todas las ideas, opiniones y contenidos expuestos en la presente investigación son de exclusiva responsabilidad de su autor.

Cuenca, 8 de septiembre de 2021

Darío Xavier Zhiña Villa

010504448-1



DEDICATORIA

A Dios por la oportunidad que me ha brindado para poder alcanzar este nuevo objetivo en mi vida.

A mi padre Manuel Zhiña, por sus consejos y el apoyo que me ha sabido brindar a lo largo de todos estos años.

A mi madre Blanca Villa, porque siempre ha estado ahí cuando lo he necesitado, por el amor que me brinda y por sus que se ven reflejados en este nuevo objetivo que lo estoy alcanzando.

A mis hermanas Daniela y Diana, que desde muy pequeñas siempre me han apoyado y han confiado en que cumpliré todas mis metas.

A mis amigos y amigas que siempre me han estado apoyando y aconsejando.



AGRADECIMIENTOS

Agradezco a Dios por la salud y vida que me ha dado para poder cumplir esta nueva meta que me he propuesto.

A mis padres Manuel y Blanca y a mis hermanas Daniela y Diana por los consejos y apoyo que me han brindado en este tiempo.

A mi director de tesis Giovanny Mosquera y mi co-director Patricio Crespo que con sus conocimientos y experiencia me han brindado todo el apoyo y orientación los cuales se ven reflejados en el trabajo de investigación.

Al proyecto “*Desarrollo de indicadores hidrológicos funcionales para la evaluación del impacto del cambio global en ecosistemas Andinos*” bajo el cual se desarrolló el trabajo de investigación.

A la Universidad de Cuenca, así como al Departamento de Recursos Hídricos y Ciencias Ambientales debido a que gracias a ellos recibí una beca para poder iniciar mis estudios de maestría.

Al programa de maestría en Hidrología con mención e Ecohidrología, ya que gracias a este programa adquirí los conocimientos necesarios para poder llevar a cabo la presente investigación.

A las personas que colaboraron en la parte de trabajo de campo y análisis de laboratorio de las muestras recolectadas para el presente estudio.

A mis amigos y amigas que siempre han estado ahí para mí, dándome ánimos y aconsejándome en todo momento.

A mis profesores de maestría que me han compartido su conocimiento a lo largo de este tiempo.



1. INTRODUCTION

Understanding the factors influencing local precipitation in mountainous regions is of scientific (meteorology, climatology, hydrology) and social relevance (economics, agriculture, cattle raising) given that these regions supply the water needs of millions of people on Earth (Ingraham, 1998; Sloat et al., 2018; Thibeault, Seth, & Wang, 2012). Acquiring this understanding can be of great help to implement and validate climate models (regional and global), obtain more realistic precipitation and climate maps, and understand how the water balance of catchments could be affected by future changes in global climate. This knowledge can also help implement adaptation strategies in areas where future changes in climate patterns and/or changes in land use can negatively affect the amount of precipitation falling in a given region. Thus, the research aimed to identify the factors that influence the isotopic composition of precipitation in mountainous regions, the origin of the water vapor masses, and the atmospheric conditions along its trajectory. The aforementioned has become a topic of major interest in atmospheric sciences (Gimeno & Beniston, 2013). However, this knowledge is still limited in mountainous regions in developing areas around the world, such as the alpine highlands of south Ecuador.

The analysis of the water stable isotopes (WSI) of oxygen-18 ($\delta^{18}\text{O}$) and hydrogen-2 (or deuterium, $\delta^2\text{H}$) in precipitation has become one of the most powerful methodologies to fill this knowledge gap in different regions around the world (Araguás-Araguás, Froehlich, & Rozanski, 2000; He, Goodkin, Jackisch, Ong, & Samanta, 2018; Kaseke, Wang, Wanke, Tian, & Lanning, 2018). These tracers provide information about the history of the water contributing to local precipitation. This is partially possible through the comparison of the global relation between $\delta^2\text{H}$ and $\delta^{18}\text{O}$ in precipitation, known as the Global Water Meteoric Line (GMWL, defined by the linear relationship: $\delta^2\text{H} = 8\delta^{18}\text{O} + 10\text{‰}$) and the Local Water Meteoric Line (LMWL, derived from the relation between both isotopes in precipitation collected at a specific site) (Craig, 1961). Differences in slope and intercept between the LMWL



relative to the GMWL can provide information about the source of moisture (e.g., continental versus maritime), moisture recycling and regional re-evaporation processes, and/or atmospheric conditions under which local precipitation forms at a given site (Kendall & McDonnell, 2012; Leibundgut, Maloszewski, & Külls, 2009). Additional information can also be obtained through the seasonal variability of ^2H and ^{18}O and the deuterium excess (D-excess, $D = \delta^2\text{H} - 8\delta^{18}\text{O}$) (Dansgaard, 1964) of each of the individual precipitation samples and their relation with local (or “in situ”) atmospheric conditions (e.g., relative humidity, air temperature, wind speed and direction, radiation, precipitation amount and type). Despite the valuable information these environmental tracers provide to better understand local precipitation, this information alone is not sufficient for understanding the factors influencing the isotopic composition of precipitation. Thus, WSIs are often used in combination with complementary methods, to obtain a complete understanding of this issue.

Complementary to the analysis of the WSI in precipitation, a variety of air mass transport models have been used to determine the pathways air masses follow from their origin to the region they condensate and precipitate. Lagrangian transport models are among the most widely used in different studies around the world (e.g., Ciric, Stojanovic, Drumond, Nieto, & Gimeno, 2016; Heydarizad, Raeisi, Sori, & Gimeno, 2019; Le Duy, Heidbüchel, Meyer, Merz, & Apel, 2018; Ricardo Sánchez-Murillo, Durán-Quesada, Birkel, Esquivel-Hernández, & Boll, 2017). In hydrometeorological and climatological studies, these types of models have helped determine the main sources of humidity contributing to local precipitation at a given study site, as well as information about their trajectory (Heydarizad et al., 2019). Lagrangian models also provide information about the “regional” meteorological conditions (e.g., temperature, relative humidity, solar radiation) that could affect the formation of precipitation. That is the atmospheric conditions to which air masses are subjected to along their pathway to the region of interest. Thus, both the identification of the origin and pathways of moisture contributing to precipitation and information about the climatological conditions that influence water vapor transport



provide valuable information to better understand the factors influencing the isotopic composition of precipitation at the study area of interest.

Several studies in different regions of the planet have used Lagrangian transport models in combination with WSI collected at different temporal resolutions (from monthly to precipitation events) (Le Duy et al., 2018; R. Sánchez-Murillo et al., 2016; Ricardo Sánchez-Murillo et al., 2017). Although the use of WSI data collected weekly or monthly is helpful to provide insights into the main moisture sources contributing to local precipitation, data collected at high-frequency (e.g., sub-daily or during rainstorm events) during at least a complete hydrological year is needed to obtain a thorough understanding of the factors influencing the isotopic composition of precipitation. The latter allows identifying potential contributions from air masses originated from different moisture sources during different times of the year. In the tropical Andes, there are only two studies that have used this approach. Windhorst, Waltz, Timbe, Frede, & Breuer (2013) used isotopic data collected at a high temporal frequency (rainstorm events) over a short period (September-December 2010) to investigate how elevation and climate variables influenced the isotopic composition of precipitation at a tropical forest site at elevations between 1800 to 2800 m a.s.l. The short study period, however, limited these authors to provide a complete understanding of how their findings are representative over a complete hydrological year. Differently, Esquivel-Hernández et al. (2018) used a data set collected during 17 months (January 2015-May 2016) at a weekly time-scale in the tropical alpine highlands (3,900 m a.s.l.) of south Ecuador. Although this study helped identify the sources of moisture contributing to local precipitation, the coarse temporal resolution of the used data limited the investigation. Different moisture sources that could also contribute to local precipitation and the factors controlling the isotopic composition of precipitation at short time scales could not be determined. Thus, a complete understanding of this research topic is still limited in the highlands of the tropical Andes.



Therefore, this study aims to use a combined analysis of isotopic data collected at high temporal frequency (during rainstorm events) and a Lagrangian transport model to identify the factors (in situ and/or regional) that influence the isotopic composition of precipitation in the tropical alpine highlands of south Ecuador. Studies of this type in the tropical Andes are necessary to understand local precipitation processes and how changes in global climate could affect them in the future.

2. MATERIALS AND METHODS

2.1 Study site

The study site is the Zhurucay Ecohydrological Observatory (ZEO, Figure1). It is situated within a tropical alpine ecosystem, known as páramo. It locates in southern Ecuador (3°04'S, 79°14'W) between 3,400 to 3,900 m a.s.l. (Mosquera, Lazo, Céleri, Wilcox, & Crespo, 2015). The climate of the study area is influenced by the continental air masses from the Amazon basin on the east, and the Pacific regime that arrives from the west (Córdova, Carrillo-Rojas, Crespo, Wilcox, & Céleri, 2015; Padrón, Wilcox, Crespo, & Céleri, 2015). Precipitation in the area is slightly bimodal, with the driest season occurring between August to September and another dry season between December to February. Mean temperature and mean annual precipitation are 6.0°C (Córdova et al., 2015) and 1,345 mm at 3,780 m a.s.l. Rainfall intensity is generally low, rarely exceeding 5 mm h⁻¹ and falling primarily as drizzle (Padrón et al., 2015). The weekly isotopic composition of precipitation is variable throughout the year and shows a seasonal pattern. That is, more depleted values are observed during the wettest months (April-May) and more enriched values during the driest months (August-September). The relationship between $\delta^2\text{H}$ and $\delta^{18}\text{O}$ composition in precipitation presents a slope of 8.37 ± 0.04 and an intercept (D-excess) of $18.04 \pm 0.39\text{‰}$ (Mosquera, Céleri, et al., 2016; Mosquera, Segura, et al., 2016).

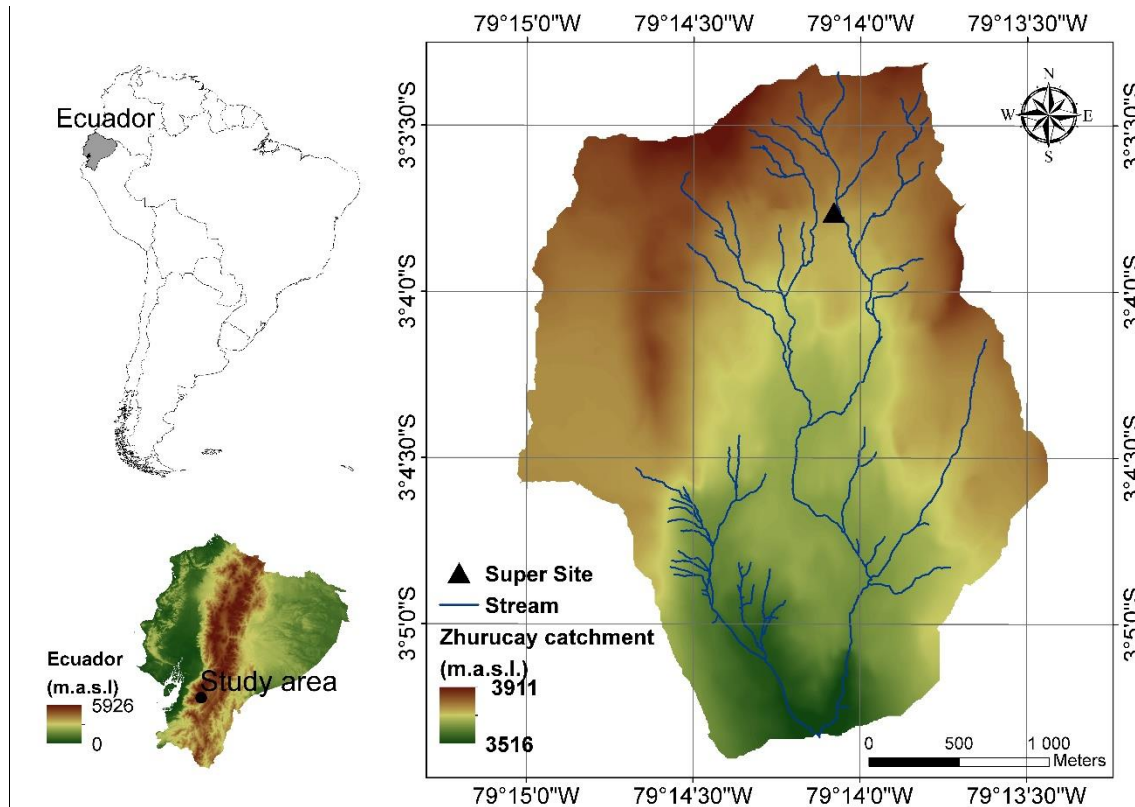


Figure 1. The Zhurucay Ecohydrological Observatory (ZEO) situated in south Ecuador. The black triangle in the map shows the location of the Super Site where the sequential sampler for collecting precipitation water samples at high temporal frequency, the meteorological station, and the disdrometer were placed.

2.2 Meteorological data collection

Meteorological data were obtained from an automatic weather station located within the ZEO Super Site (Figure 1). Air temperature and relative humidity were measured by a Campbell Scientific CS-215 probe. Wind speed was measured using a Met-One 034B Windset anemometer. Solar radiation was measured using an Apogee CS300 pyranometer. For the collection of precipitation data, a TEXAS tipping bucket rain gauge with a resolution of 0.1 mm was used. These variables were recorded every 5 minutes. These data were used as used as possible “in situ factors” factors that could influence the temporal variability of the isotopic composition of precipitation.



The fractions of different types of rain occurring in the study area were also determined. For this purpose, data from a disdrometer (Thies Clima, 2007) located within the ZEO Super Site (Figure 1) was used. This is a laser sensor that produces a horizontal light strip and when the precipitation particle falls through the light beam, the signal is attenuated and the diameter of the raindrop (D_m) can be estimated from the reduction in amplitude of the signal attenuated. The disdrometer operates at a wavelength of 785 nm and has a reference measurement area of 45.6 cm² and a resolution of 0.005 mm h⁻¹. The methodology described by Orellana-Alvear, Céleri, Rollenbeck, & Bendix (2017) was followed to classify different types of rain and their respective fractions during different time periods of interest. The threshold values considered to classify rainfall according to its drop diameter (D_m) were: $0.1 < D_m$ (mm) ≤ 0.5 ; $0.5 < D_m$ (mm) ≤ 1.0 ; $1.0 < D_m$ (mm) ≤ 2 ; $2 < D_m$ (mm) and in this way rainfall was classified as light (L), moderate (M), heavy (H) and very heavy (VH), respectively, and its respective contributions to total precipitation were also estimated. The fractions of each rainfall type were also used as potential controls on the stable isotopic composition of precipitation.

2.3. Isotopic data collection and laboratory analysis

Precipitation water samples for stable isotopes analysis were collected during rainfall events at the SuperSite of the ZEO (Figure 1) during the period October 2017 – November 2018 (n = 295). Sampling was carried out using a hand-made sequential rainfall sampler (Figure A1 from supplementary material). The sequential sampler consisted of two circular funnels of 25 cm diameter connected by tubes (rigid polycarbonate tubing 6 mm of internal diameter x 9 mm outside diameter) to ten glass bottles of 0.5Lt connected in series using Y-connectors (Figure A1b from supplementary material). The glass bottles were placed inside a wooden structure lined with batting cotton and aluminum foil. This structure isolated the bottles from the surrounding heat and thus prevented changes in the isotopic composition of rainfall samples due to evaporation.



The principle of operation of the sequential rainfall sampler based on a balance of pressures, in which water filled a bottle until a certain pressure was reached (i.e., atmospheric pressure). At this stage, water is diverted to another bottle and in this way, it is possible to obtain sequential samples of an entire precipitation event (McDonnell, Bonell, Stewart, & Pearce, 1990). Each bottle collected 160 ml of water, corresponding to 2.08 mm of rainfall. Precipitation data from a rain gauge located 3 m from the sequential sampler was used to determine the time at which each bottle was filled with water. Precipitation was collected and stored in 2 mL amber glass bottles. The use of a thin layer of mineral oil in the rainfall collector is recommended to avoid fractionation by evaporation (Mook & Rozanski, 2000). However, mineral oil was not used in this study because evaporation did not affected the water samples. This was verified during a test period of the sequential sampler carried out 3 months before the start of this study without using mineral oil. All of the samples collected during the test period were plotted in the $\delta^2\text{H}$ - $\delta^{18}\text{O}$ dual space and compared to the historical LMWL (2011-2018) of the study site, showing that evaporation did not affect their isotopic composition (i.e., no samples plotted outside the expected values for the isotopic composition of precipitation). The collected samples were covered with parafilm and kept away from the sunlight until analysis to prevent fractionation by evaporation during transport and storage until their analysis in the laboratory (IAEA, 2014; Mook & Rozanski, 2000).

The isotopic composition of the precipitation samples was measured in the Water Quality Laboratory of the Department of Water Resources and Environmental Sciences of the University of Cuenca using a cavity ring-down spectrometer L1102-i Picarro. The instrument has a 0.5‰ precision for deuterium ($\delta^2\text{H}$) and 0.1‰ precision for oxygen-18 ($\delta^{18}\text{O}$). At the suggestion of the manufacturer and for the reduction of the memory effect in the analyses (Penna et al., 2012), six injections of the sample were applied and the first three were discarded. For the last three injections, the difference between the maximum $\delta^{18}\text{O}$ isotopic composition was calculated and compared with the analytical accuracy given by the manufacturer and



the standard deviation of the isotopic standards used for the analysis. Samples with larger differences were re-analyzed. Organic contamination of the isotopic composition was verified through the use of the ChemCorrect 1.2.0 software (Picarro, 2010). Stable isotope compositions are reported in delta notation δ (‰, per mil) relative to the Vienna Standard Mean Ocean Water (V-SMOW; Craig, 1961).

2.4. Origin and trajectories of water vapor masses

The origin and trajectory of water vapor masses were determined through the generation of backward trajectories based on the Hybrid Single-Particle Lagrangian Integrated Trajectory (HYSPLIT) model developed by NOAA (Draxler & Hess, 1998; Stein et al., 2015). The HYSPLIT model determines the position of water vapor masses using a three-dimensional Lagrangian velocity algorithm of air masses (Stein et al., 2015). The input data needed by the HYSPLIT model corresponds to the variables of pressure, temperature, wind speed, and solar radiation obtained from the NOAA meteorological database [GDAS, global data assimilation system: 2006-present; 0.5° resolution, (Rolph, Stein, & Stunder, 2017; Su, Yuan, Fung, & Lau, 2015)]. For each precipitation sample collected, a backward trajectory was calculated. Backward trajectories were calculated for periods of 192 hours (eight days) at 1-hour interval. The calculation time was selected according to the expected residence time of water in the atmosphere [4-10 days (Van Der Ent & Tuinenburg, 2017)]. In addition, a height of 3,800 m a.s.l. (633 mb) was chosen for the start of the backward trajectory. This height corresponds to the probable height of the cloud base (Esquivel-Hernández et al., 2019; Lawrence, 2005). The HYSPLIT model provides information about the variables that influence the determined air moisture trajectories. These variables include potential temperature, ambient temperature, precipitation rate, relative humidity, solar radiation, pressure, mix depth, and altitude of the air parcel. These meteorological variables were used as potential “regional” factors controlling the isotopic composition of precipitation.

Trajectories of the air masses transporting precipitation were analyzed based on the regions considered as sources of atmospheric humidity through which they travelled before reaching the study area. These regions were defined based on the study by Agudelo, Arias, Vieira, & Martínez (2018). The sources of atmospheric humidity considered included 17 regions (as shown in Figure 2): five ocean and 12 continental regions.

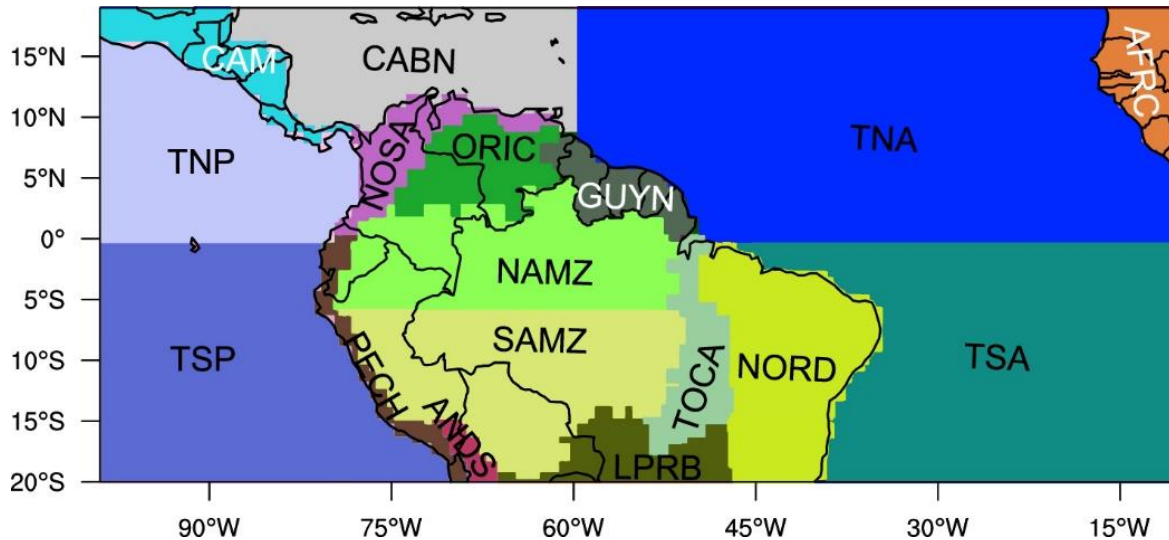


Figure 2. Regions considered as sources of moisture through which the air masses travel before reaching the study area. The 17 regions correspond to: Central America (CAM), Northern South America (NOSA), Orinoco basin (ORIC), Guyanas (GUYN), Peru–Chile (PECH), Northern Amazon (NAMZ), Southern Amazon (SAMZ), Subtropical Andes (ANDS), Tocantins basin (TOCA), La Plata River Basin (LPRB), Brazil’s Northeast (NORD), Africa (AFRC), Tropical North Pacific (TNP), Tropical South Pacific (TSP), Caribbean Sea (CABN), Tropical North Atlantic (TNA), Tropical South Atlantic (TSA). Figure adapted from Ruiz-Vásquez, Arias, Martínez, & Espinoza (2020.)

2.5. LMWL and D-excess analysis

The LMWL analysis was carried out by comparing the slopes and intersections of the LMWL of the study site and the GMWL. When comparing both lines, it could be identified if there are re-evaporation processes affecting local precipitation (as a result of the evaporation of rain or water intercepted in the vegetation canopy) (Benjamin, Knobel, Hall, Cecil, & Green, 2004; Liebming, Haberhauer, Papesch, & Heiss, 2006; Noone, 2012; Putman, Fiorella, Bowen, & Cai, 2019). The construction of the LMWL was carried out by linear regression using the isotopic



composition data of $\delta^{18}\text{O}$ and $\delta^2\text{H}$ from precipitation samples and the adjustment of the LMWL was assessed using the coefficient of determination R^2 . Also, an analysis of D-excess ($D = \delta^2\text{H} - 8\delta^{18}\text{O}$) was conducted to identify moisture recycling processes from the Earth's surface due to the transpiration of plants and water evaporated from surface water bodies. High values of D indicate that local precipitation was composed of recycled moisture (K. Froehlich, Gibson, & Aggarwal, 2002; Klaus Froehlich et al., 2008; Pang et al., 2011; Salati, Dall'Olio, Matsui, & Gat, 1979).

2.6. Analysis of factors controlling the isotopic composition of precipitation

Given that the stable isotopic composition of precipitation at a given site depends on the origin and transport of atmospheric moisture, as well as in situ meteorological conditions, the analysis was carried out through the use of isotopic composition ($\delta^{18}\text{O}$, $\delta^2\text{H}$, and D-excess) and local (in situ) and regional meteorological variables.

In situ factors included the meteorological variables measured at the climate station located at the ZEO Super Site (Figure 1). These variables were: accumulated precipitation (Prec_i), average values of temperature (Temp_i), relative humidity (RH_i), wind speed (WS_i), atmospheric pressure (Press_i), and solar radiation (SR_i) corresponding to the sampling period of each of the collected samples. Also, the fractions of the different rainfall types occurring in the study area were considered as possible controlling factors. That is, Light (L), Moderate (M), Heavy (H), Very Heavy (VH) rainfall, and several combinations among those fractions: L+M, M+H, H+VH, L+M+H, and M+H+VH.

Regional factors included the meteorological variables along the trajectory of the water vapor masses generated from the HYSPLIT model. The outputs from the model correspond to rainfall rate along the trajectory (Prec_x), trajectory altitude (Alt_x), air temperature (Temp_x), potential temperature (PT_x), mix depth (MD_x), pressure (Press_x), downward solar radiation flux (SR_x), and relative humidity (RH_x). As the model produces hourly outputs of this information along the determined air mass trajectories, the average values from one to eight days backward (the subscript "x")



after each of the regional variables indicates the corresponding backward day) were used to investigate whether these regional variables influence the isotopic composition of local precipitation.

The analysis of the factors influencing the isotopic composition of precipitation comprised a series of steps (Figure A2 from supplementary material). First, a multicollinearity analysis among the in situ and regional variables was performed to remove redundant information that may affect the statistical analyses. The criteria used for this purpose was the Variance Factor Index (VIF) (Lin, Foster, & Ungar, 2011) considering a threshold value of 3 (Hair Jr, Hult, Ringle, & Sarstedt, 2016). Subsequently, a Spearman's correlation analysis was performed using the variables yielded from the VIF analysis and the values of isotopic composition of precipitation. If high correlation values were obtained ($r \geq 0.7$), simple linear regression (SLR) models were developed between these variables and the isotopic composition of precipitation. Variables producing $R^2 \geq 0.5$ were considered as drivers of the isotopic composition of precipitation. If high correlation values ($r < 0.7$) were not obtained, the next step was to apply multiple linear regression (MLR) models between the factors (local and regional) and the isotopic composition of precipitation using the bidirectional stepwise criteria and examining models up to 5 variables. The evaluation of these models was carried out using the R^2_{adj} and RMSE metrics. The variables producing models that comply with having a value of $R^2_{adj} \geq 0.5$ and an $RMSE \leq 15\%$ of the isotopic variability in the analyzed dataset were considered as controllers of the isotopic composition of precipitation.

Initially, the aforementioned procedure was applied to the complete isotopic dataset. Given that no controllers of the isotopic composition of precipitation could be identified using the whole data (Section 3.3), the dataset was divided by periods: DJF (December-February), MAM (March-May), JJA (June-August), and SON (September-November), and by the predominant air mass trajectories identified by the HYSPLIT model (Section 3.2).

3. RESULTS

3.1 Description of meteorological conditions

As can be seen in Figure 3, the accumulated precipitation for each time period a water sample for isotope analysis was collected (Figure 3a) presented two dry seasons (December-February and July-September). The analysis of the precipitation type and fraction showed that most of the time precipitation is classified as light ($0.1 < D_m \text{ (mm)} \leq 0.5$), followed by moderate ($0.5 < D_m \text{ (mm)} \leq 1.0$) and heavy precipitation ($1.0 < D_m \text{ (mm)} \leq 2$; Figure 3b). On very few occasions the presence of very heavy precipitation was observed ($1.0 < D_m \text{ (mm)} \leq 2$). Regarding the average air temperature for each isotope sample (Figure 3c), it was observed that in the rainiest periods (March-May and October-November) the temperature was higher than in the dry periods (July-September). The average relative humidity for each sample was mostly above 90% (Figure 3d). In the rainiest periods (March-May) the average wind speed was low in comparison to the driest months (July-September) when it was higher (Figure 3e). Regarding solar radiation, it was low during dry periods (July-September and December-February), while it was high during the rainiest months (March-May).

3.2 Isotopic composition

The isotopic composition of precipitation at the study site varied between -2.42‰ and -24.98‰ (with a mean of -11.92‰) for $\delta^{18}\text{O}$, -0.01‰ and -184.96‰ (with a mean of -80.41‰) for $\delta^2\text{H}$, and 8.03‰ and 21.37‰ (with a mean of 15.01‰) for D-excess (Figure 3a-b). The most depleted $\delta^{18}\text{O}$ and $\delta^2\text{H}$ compositions were observed during the rainy season (March-May; Figure 3a), with enriched isotope values observed during the rest of the study period. No clear seasonal variation was observed for D-excess. Despite having analyzed the abundance of $\delta^{18}\text{O}$, $\delta^2\text{H}$, and D-excess, in the following only results obtained using the abundance of $\delta^{18}\text{O}$ and D-excess are presented because the results obtained with both isotopes ($\delta^{18}\text{O}$ and $\delta^2\text{H}$) show similar trends. The slope of the LMWL (8.15) was similar to the one of the GMWL (8; Figure 4). On the contrary, the intercept of the LMWL (16.87‰) was larger than that of the GMWL (10‰).

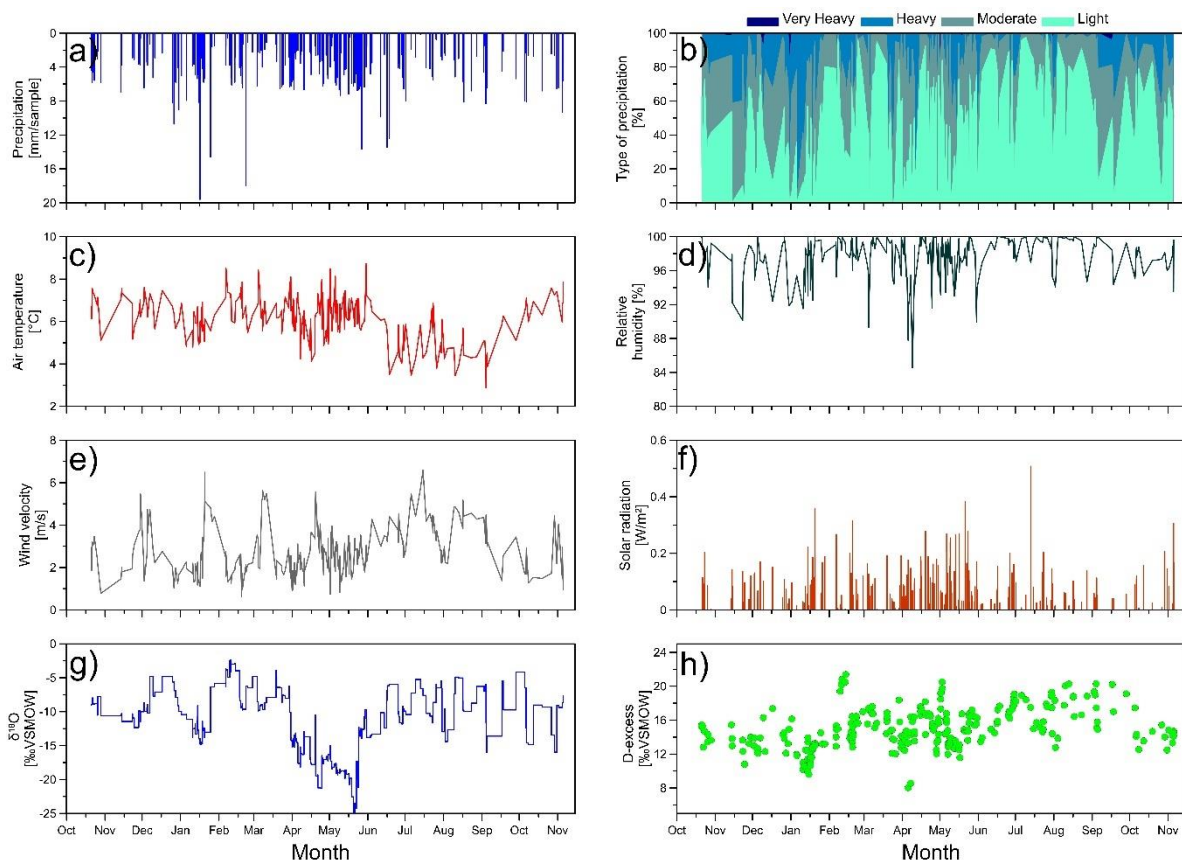


Figure 3. Time series of meteorological in situ variables: a) precipitation, b) type and fraction of precipitation, c) air temperature, d) relative humidity, e) wind velocity, f) solar radiation. Time series of isotopic composition g) $\delta^{18}\text{O}$ and h) D-excess for the period October 2017 – November 2018 at the Zhuruca Ecohydrological Observatory. **Note.** The values in Figure 3a-b represent the accumulated precipitation value and type and fraction of precipitation during the period for which each water sample for isotope analysis was collected. The values in Figure 3c-f represents the average value of local (in-situ) meteorological variables during the period for which each water sample for isotope analysis was collected.

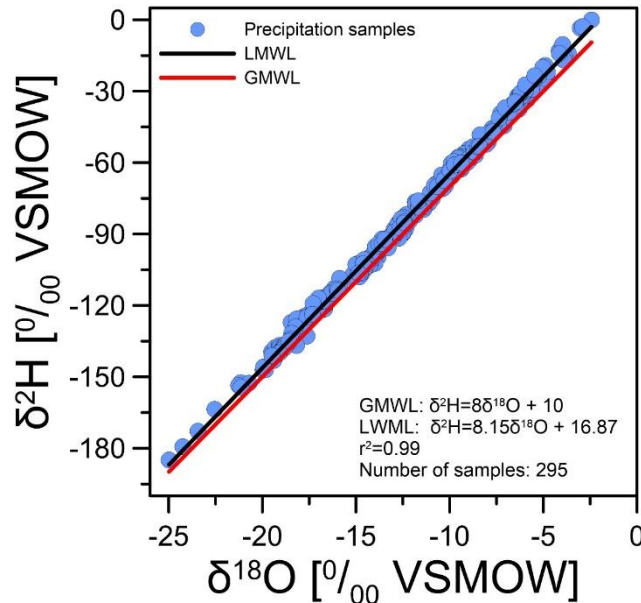


Figure 4. $\delta^2\text{H} - \delta^{18}\text{O}$ diagram constructed with the precipitation samples collected during October 2017 – November 2018. The black linear fit indicates the Local Meteoric Water Line (LMWL) based on the samples presented in the study and the red linear fit indicates the Global Meteoric Water Line [GMWL, (Dansgaard, 1964)].

3.3 Origin and trajectories of water vapor masses

The 295 trajectories of the air masses that transport precipitation to the study site are shown in Figure 5. From these trajectories, it is observed that the air masses follow four main trajectories before reaching the study area (Orinoco plains, Amazon basin, Mato Grosso Massif, and the Pacific coast). During the entire study period, it was found that 73.22% of the time the study area receives air masses originated from the Amazon basin, 11.19% of the time the masses of air cross the Orinoco plains, and with 12.88% and 2.71% of the time the air masses that transport the precipitation come from the Pacific coast and Mato Grosso massif, respectively.

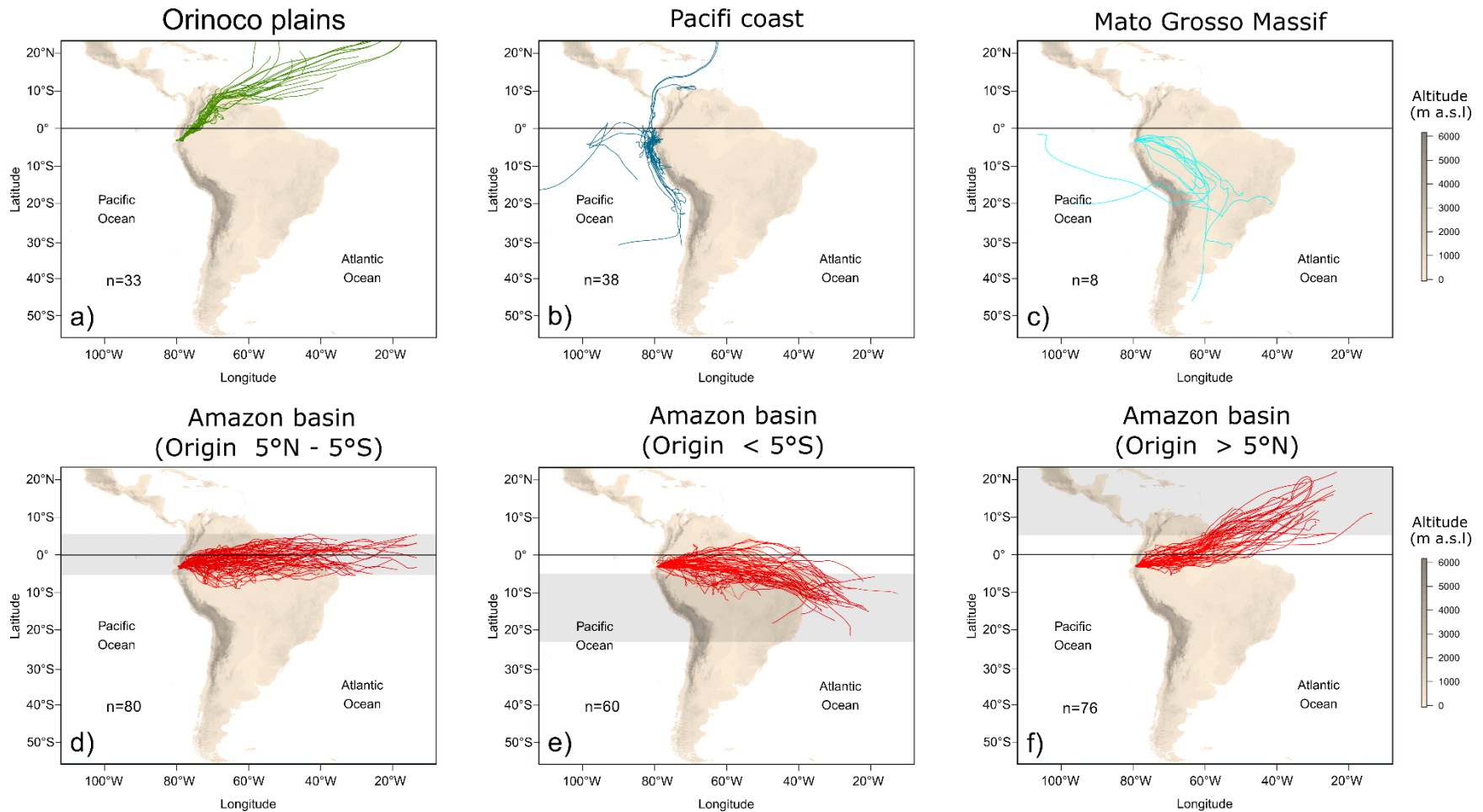


Figure 5. In the upper part of the plot are the maps with the trajectories of the air masses corresponding to the trajectories of: a) Orinoco plains, b) Pacific coast and c) Mato Grosso Massif. The lower part of the plot shows the trajectories of the air masses corresponding to the Amazon basin and subclassified according to their origin: d) trajectories of the Amazon basin with an origin between 5° N and 5° S, e) trajectories of the Amazon basin with an origin less than 5° S and f) trajectories of the Amazon basin with an origin above than 5° N. **Note:** n=number of samples for each trajectory.



Figure 5 also reveals that the air masses that transport precipitation before reaching the study site crossed the different regions (both oceanic and continental) considered as sources of atmospheric humidity presented in Figure 2. The air masses that cross the Orinoco plains had their origin in the Tropical North Atlantic region (TNA), then they advanced until they crossed the entire Orinoco basin (ORIC), continued through the northwestern part of the Northern Amazon region (NAMZ) crossing the southern part of Colombia and the northeastern region of Ecuador to reach the study area through the Andes [northern part of the Peru–Chile region (PECH)].

The air masses crossing the Pacific coast had two different regions of origin. The first group of air masses originated from the CABN region, crossed the southern part of Central America (CAM region) to the Pacific Ocean, descend through the northern of TNP, and reached the study area at the northern part of the PECH region. The second group of air masses originated in the Pacific Ocean in the Tropical South Pacific (TSP) region, ascended along the coasts of Chile and Peru (through the PECH region), and then reached the study area

The air masses that cross the Mato Grosso Massif had their origin in two regions: La Plata River Basin (LPRB) and Brazil's Northeast (NORD, and to reach the study area they crossed the region of TOCA, then ascended through the SAMZ region and finally the southern part of NAMZ.

Concerning the air masses of the Amazon basin, the air masses originating between latitudes 5°N - 5°S were originated in the middle of the Atlantic Ocean in the TNA and TSA regions. Then they cross the Atlantic Ocean until they reach the coasts of South America. Once the air masses reach the continent, they cross the northern part of the NORD and TOCA regions as well as the southern part of GUYN and continue their trajectory through the Amazon rainforest in the NAMZ region before reaching the study area.

The air masses of the Amazon basin that originated at latitudes above 5 ° N had their origin in the central part of the Atlantic Ocean in the TNA region and crossed the ocean until they reached the continent, crossing the Guyana (GUYN) zone and reaching the NAMZ region in the northeastern part, which they crossed before converging in the study area.

The air masses of the Amazon basin whose origin started below 5°S, likewise, originated in the middle of the Atlantic Ocean in the TSA region. Then, they crossed the ocean until they reached the coasts of South America. Once there, they crossed the NORD region continuing through the TOCA and SAMZ regions. Subsequently,



they ascended through the south of the NAMZ region, crossing it and arriving at the study site.

3.4 Factors controlling the isotopic composition of precipitation

A total of 80 meteorological variables (local and regional) were obtained and with these variables a multicollinearity analysis was performed using the VIF criterion with a threshold of 3. The analysis was carried out both for the entire period as well as for each season and according to each of the main air mass trajectories determined by the HYSPLIT model. After the VIF analysis, a reduction of potential controlling variables was achieved, thus having for each case: complete period (36 variables), DJF season (26 variables), MAM season (34 variables), JJA season (23 variables), SON season (21 variables), Orinoco plains (22 variables), Pacific ocean (20 variables), Mato Grosso (11 variables), trajectories of the Amazon basin with origin between 5°N and 5°S (27 variables), trajectories of the Amazon basin with origin below 5°S (25 variables), and trajectories of the Amazon basin with origin above 5° N (27 variables). These meteorological variables together with the $\delta^{18}\text{O}$ and D-excess composition were used to perform the correlation and linear regression analyses.

Results of performing Spearman correlation for the full period utilizing the isotopic signal ($\delta^{18}\text{O}$ and D-excess) and the meteorological variables (in situ and regional) showed very low correlation values ($r < 0.7$). Due to the low values found when performing this analysis, the next step was to perform multiple regression models (MLR) taking into account the four different seasons (previously described in Section 2.6) and the whole period. However, the explanation of the variance of the MLRs was less than 50% for both $\delta^{18}\text{O}$ and D-excess.

Therefore, the next step was to perform MLR on the data set, taking into account as a criterion the trajectories followed by the air masses contributing to local precipitation (Orinoco plains, Pacific coast, Mato Grosso Massif, and Amazon basin). In the case of the Amazon basin trajectories, it was necessary to further consider their origin since no MLR explaining more than 50% of the dataset variance were identified. The dataset was divided into three origins considering their position with respect to the equator as follows: trajectories with origin above 5°N, between 5°N and 5°S, and below 5°S. The main results of the MLR are shown in Table 1 and Figure 6 for brevity (the results of all the models, i.e., from one to five variables are presented in the supplementary material section).

As shown in Table 1, it was possible to find controllers for the Orinoco plains, Pacific coast, Mato Grosso Massif, Amazon between 5°N and 5°S, and below 5°S



trajectories using the datasets obtained during the whole study period. However, for the air masses that cross the Amazon basin whose origin was above than 5°N no controllers were identified. For this reason, we separated those trajectories by seasons (DJF, MAM, JJA, and SON), thus obtaining the controllers for each period, except for the JJA season, which we could not evaluate because there were too few samples to perform the analysis (less than five samples).

Concerning the isotopic signal of $\delta^{18}\text{O}$ for the air masses crossing the Orinoco plains, we found two drivers (Temp_i and Prec_5) which explained 60% of the variance. In the case of the air masses crossing the Pacific coast, four controllers were found (M+H+VH , Prec_1 , RH_8 , and RH_6) that explains 58.1% of the variance. For the air masses of Mato Grosso, variables RH_i , Prec_4 and SRad_i were able to explain 93% of the variance of the system. However, something that should be considered is that there were only eight samples that corresponded to this trajectory. For air masses of the Amazon basin that originated between 5°N and 5°S, four drivers (MD_4 , Prec_7 , Prec_6 , Prec_3) were obtained to explain 56.2% of the variance. Air masses with origin below 5°S and crossing the Amazon basin exhibited four drivers (Temp_i , Press_i , RH_6 , and H+VH) which explained 53.4% of the variance of the isotopic composition of precipitation.

Regarding the air masses of the Amazon basin with an origin higher than 5N, it was not possible to obtain isotopic composition drivers that explain a minimum of 50% of the variance, as can be seen in Table 1. Thus, we divided these trajectories into seasons (DJF, MAM, JJA, and SON). In DJF, three variables (SRad_1 , Temp_i , and SRad_2) explained 58.4% of the variance from the isotopic signal. Only two variables (Press_i and RH_3) were necessary to explain more than half of the variance of the isotopic signal (54.4%) for MAM. No controllers were found for JJA due to the number of samples being too small to perform MLR (less than 5 samples). For SON, a single variable (HR_2) was required to explain more than half of the isotopic signal of the system (66.6%).

For the D-excess, it is not possible to define clear controllers able to explain at least 50% of the variance, neither by dividing the isotopic signal by season nor by dividing it by the origin of their trajectories (the results of the analysis can be found in the supplementary material section).

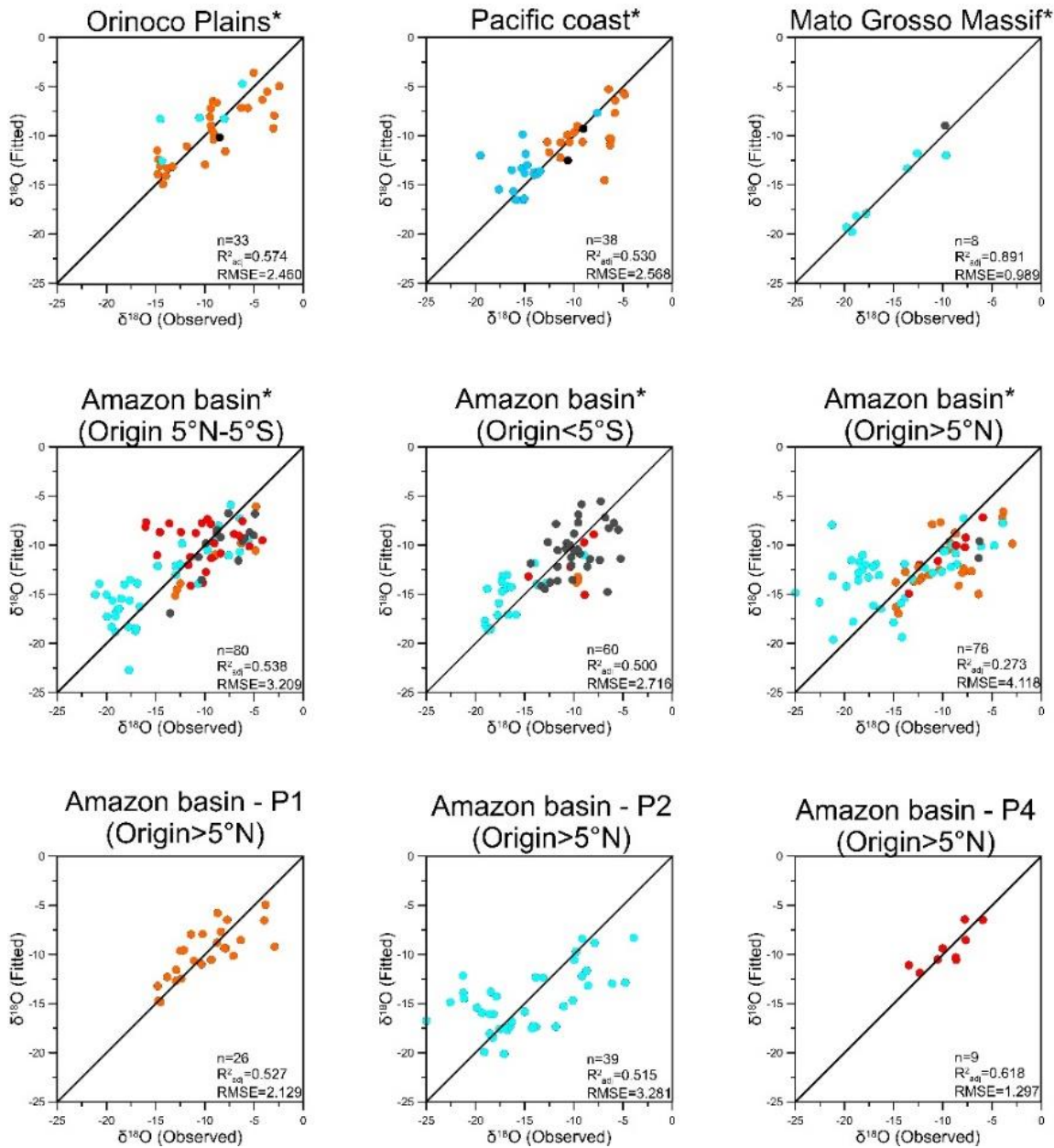


Figure 6. X-Y graph of the observed and simulated isotopic composition of $\delta^{18}O$ with the Multiple Linear Regression (MLR) for their respective trajectories. **Note:** n=number of samples, R^2_{adj} = Adjusted R-squared, RMSE = Root Mean Square Error and * indicates that samples collected during the whole year were included for the MLR.

**Table 1.** Results of performing the Multiple Linear Regression (MLR) for $\delta^{18}\text{O}$ after using the stepwise criterion

Trayectorias	Variables	n	m	R ²	R ² _{aj}	AIC	RMSE	pVal
Orinoco plains	Temp _i , Prec ₅	33	2	0.601	0.574	161.061	2.460	1.05E-06
Pacific coast	M+H+VH, Prec ₁ , RH ₈ , RH ₆	38	4	0.581	0.530	191.511	2.568	6.27E-06
Mato Grosso Massif	RH _i , Prec ₄ , SRad _i	8	3	0.938	0.891	32.538	0.989	7.08E-03
Amazon basin (5°N - 5°S)	MD ₄ , Prec ₇ , Prec ₆ , Prec ₃	80	4	0.562	0.538	425.569	3.209	8.09E-13
Amazon basin <5S	Temp _i , Press _i , RH ₆ , H+VH	60	4	0.534	0.500	327.392	2.716	2.15E-08
Amazon basin >5N	Prec ₂ , RH ₂ , RH ₃ , Prec ₆ , Temp _i	76	5	0.321	0.273	444.830	4.118	4.23E-05
Amazon basin >5N - P1	SRad ₁ , Temp _i , SRad ₂	26	3	0.584	0.527	123.073	2.129	1.97E-04
Amazon basin >5N - P2	Press _i , RH ₃ ,	39	2	0.544	0.515	229.810	3.281	4.53E-04
Amazon basin >5N - P4	RH ₂	9	1	0.666	0.618	36.224	1.297	7.29E-03

Note: Insitu variables: Temp_i (Air temperature), Press_i (Pressure), RH_i (Relative humidity), SRad_i (Solar radiation), H+VH (accumulated fraction of heavy and very heavy precipitation), M+H+VH (accumulated fraction of moderate, heavy and very heavy precipitation), **Regional variables:** MD (Mix Depth), SRad_x (Solar radiation), Prec_x (Precipitation), RH_x (Relative Humidity). The number next to the regional variable indicates the day backward. n = number of samples used for the MLRs, m = number of variables used to obtain the MLRs, R² = R-squared, R²_{aj} = Adjusted R-squared, AIC = Akaike



4. DISCUSSION

4.1 Isotopic composition

The range of isotopic composition was very wide. Depleted values of $\delta^{18}\text{O}$ and $\delta^2\text{H}$ during wet periods and enriched during dry periods are similar to those found in studies of Esquivel-Hernández et al. (2019) and Mosquera et al. (2016) developed in the Andean páramos of southern Ecuador. The depleted values may be due to the passage of the ITCZ over the Ecuadorian Andes and the Amazon basin and related to the convective activity of the region (Gastmans et al., 2017; K Rozanski & Araguas, 1995). On the other hand, the enriched values may be due to the recycling of moisture that comes from the Ecuadorian Amazon. This moisture is less influenced by local reevaporation of the sub-cloud due to the short distance between the base of the cloud and the Andes and also by the low moisture saturation deficit due to high air humidity throughout the year in the study area [with an annual average of 92% (Esquivel-Hernández et al., 2019; Muñoz, Céleri, & Feyen, 2016)]

The slope of the LMWL (8.13) was not significantly different than the GMWL (8), indicating that fractionation by evaporation of raindrops does not occur in the páramo ecosystem, as has been observed in other ecosystems (Dinçer & Payne, 1971). The larger intercept of the LMWL (16.59) compared to the GMWL (8) could have two possible explanations. The first one is because the water vapor, although it has different trajectories, (for about 86 % of the events it crosses the Orinoco, Guiana, and Amazon areas) before reaching the study site, finally converge near the Amazon rainforest. As they ascend the mountain range, they would undergo isotopic fractionation under non-equilibrium conditions, due to the process of re-evaporation of precipitation and recycling of moisture during their passage through the Amazon rainforest. The study developed by Gastmans et al. (2017) presented similar variations in LMWL interception (between + 12 ‰ and 13 ‰) at stations located in Belo Horizonte, Rio de Janeiro, Campo Grande, Rio Claro, and Betânia (located along the Amazon forest) and was attributed to water vapor recirculation. The second explanation, in the same way as indicated by the study of Esquivel-Hernández et al. (2019) is that maybe the water vapor that originates in the Pacific Ocean, when it is transported from the ocean to the Ecuadorian coast (where temperatures are commonly above 20°C), and the n begins to rise to the colder regions of the Ecuadorian Andes, it suffers a strong fractionations under non equilibrium conditions.



4.2 Origin and trajectories of water vapor masses

The air masses from the eastern side of the mountain range contributed to 86% of the precipitation that reached the study site. This agrees with other studies that indicate that both the Atlantic Ocean and the Amazon forest are the main sources of humidity for the northern tropical Andes (Arias, Martínez, & Vieira, 2015; Espinoza et al., 2020). On the other hand, the air masses that come from the western part (Pacific Ocean) have a low contribution (15.59%), which agrees with the study of Esquivel-Hernández et al. (2019) in which a small percentage of the air masses that transported moisture and precipitation to the Andean páramo of Southern Ecuador had their origin in the Pacific Ocean.

All these water vapor air masses, regardless of their origin and trajectory, are affected by different Low-Level Jets (LLJ), which transport large amounts of moisture in South America. Among these LLJs, we have the Orinoco Low-Level Jet (OLLJ; Jiménez-Sánchez, Markowski, Young, & Stensrud, 2020) which influences the air masses that cross the Orinoco plains. Air masses from the Pacific coast are influenced by the Chocó low-level jet dynamics (Arias et al., 2015; Sakamoto, 2011) that is a product of atmosphere-ocean-land connections, which then rise by orographic effect from the tropical Andes to interact with the warmer trade winds from the east of the mountain range. Air masses coming from both the Guiana massif and the Amazon rainforest are affected by the South American low-level jet (SALLJ) in which the water vapor entering the Amazon River basin mixes with the locally recycled water thus increasing the moisture available for precipitation. (Montini L., Jones, & Carvalho, 2019; Poveda, Jaramillo, & Vallejo, 2014).

The results obtained from the trajectories of the water vapor masses in the present study are similar to other studies such as those of (Esquivel-Hernández et al., 2019; Windhorst et al., 2013) developed in the Andes. This fact provides confidence that the Lagrangian models used to track humidity patterns are adequate for these types of studies.

4.3 Factors controlling the isotopic composition of precipitation

Various factors have been found in the literature to control the isotopic composition of precipitation, from the first studies carried out by (Dansgaard, 1964) to more recent others carried out in several regions of the world and various ecosystems (Kattan, 2019; Le Duy et al., 2018; K Rozanski & Araguas, 1995; Kazimierz Rozanski, Araguás-Araguás, & Gonfiantini, 1993; R. Sánchez-Murillo et al., 2016;



Windhorst et al., 2013). However, in the Andean region, this type of study has not been carried out at a scale as detailed as the one in the present study, which is of precipitation events. This can provide a greater understanding of what type of factors control the isotopic composition of precipitation.

Regional factors in all the trajectories that were identified explain most of the variance of the isotopic composition of their corresponding precipitation samples. The changes in the interception of LMWL concerning the GMWL are mostly due to re-evaporation processes of precipitation and moisture recycling that take place in previous days when the air masses are generated both over the Amazon basin as well as over the Orinoco basin. The regional variables resulting from the MLR are variables that when analyzed are located on certain regions where the aforementioned processes occur.

The isotopic composition of precipitation samples corresponding to the Orinoco plains (Figure 5) are controlled by two factors, $Temp_i$ and $Prec_5$. Local (in situ) temperature has been found to be a factor that controls the isotopic composition (Dansgaard, 1964; Kattan, 2019; Le Duy et al., 2018), so it could be expected for this variable to be present as a controller. On the other hand, the air masses that cross the Orinoco plains are affected by the OLLJ, as seen in Figure 6, most of the precipitation samples correspond to the DJF season in which the OLLJ is most active, and the place where the OLLJ originates according to (Jiménez-Sánchez et al., 2020) corresponds to the place where the air masses were 5 days back, which explains the fact that $Prec_5$ is a predictor in the MLR model.

The main variables influencing precipitation isotopic composition corresponding to the Pacific coast were $M+H+VH$, $Prec_1$, HR_8 , and HR_6 . These air masses that transport precipitation are influenced by the CHOCO jet, which is associated with Mesoscale Convective Systems (MCS) that cause heavy rains (Poveda et al., 2014), which would explain the presence of the variable $M+H+VH$ in the MLR model. Also, the study area seems to produce more convective activity due to the presence of higher thermal breeze and moist air advection (Orellana-Alvear et al., 2017), which reaffirms the presence of the variable $M+H+VH$ in the MLR. Previous studies, for example those of (Kurita, 2013; Nlend et al., 2020; R. Sánchez-Murillo et al., 2016), similarly mention convective processes as factors controlling the isotopic composition of precipitation in the tropics. Moisture transport by the CHOCO jet can be traced back as far south as $30^{\circ}S$ (Poveda et al., 2014; Sakamoto, 2011) which corresponds to the coasts of Chile and may explain the presence of the variables HR_8 and HR_6 in the MLR model. The CHOCO jet is weaker from December to March and it veers to Ecuador during that time of the year (Poveda et al., 2014), it also



brings more rainfall to the area around the equator from December to March (Poveda et al., 2014). This coincides with the fact that most samples from the Pacific trajectory are collected during these months (Figure 6).

The isotopic composition of precipitation samples whose trajectory crossed the Mato Grosso massif presented the variables HR_i , $SRadi_i$, and $Prec_4$ as controllers. The first two are in situ meteorological variables, that have been identified as controllers of the isotopic composition in previous studies (Kattan, 2019; Le Duy et al., 2018). While $Prec_4$ would indicate that the precipitation of 4 days backward, when the air masses are over the SAMZ zone (Figure 2,) it is a controller.

For the air masses that transport precipitation whose trajectory crosses the Amazon basin and has its origin between the coordinates $5^\circ N$ - $5^\circ S$, four controllers were found that were regional variables (MD_4 , $Prec_7$, $Prec_6$, and $Prec_3$). The humidity that is generated in the Atlantic Ocean and forms precipitation ($Prec_6$ and $Prec_7$) is transported to the continent by the trade winds. It then crosses the Amazon rainforest in which the convection and turbulence processes give rise to the mixture of the masses of air (MD_4) with humidity ($Prec_3$) product of the photosynthetic activity of the area which reaches its peaks from May to November (Doughty & Goulden, 2008). This coincides with the fact that most of the precipitation samples correspond to this period, then the air masses reach the east of the Andes and ascend until they reach the study area. This means that the processes of moisture transport few days before rainfall reaches the study area from the Tropical Atlantic through the Amazon basin into the Andean cordillera are important to explain the isotopic composition of local precipitation.

The isotopic composition of the precipitation samples from the Amazon basin whose origin is south of $5^\circ S$ presented four controllers ($Temp_i$, $Press_i$, $H+VH$, and HR_6). The in situ temperature has sometimes been found as a controller of the isotopic composition of precipitation (Kattan, 2019; Le Duy et al., 2018), which explains its presence as a predictor in the MLR model. $Press_i$ could be indirectly related to the temperature of the area, which is a controller according to the literature (Dansgaard, 1964), due to the decrease in temperature due to an adiabatic lapse rate caused only by the change in pressure (Ingraham, 1998; Rindsberger, M. Magaritz, & Gilad, 1983). The variable $H+VH$ refers to the type of rain which is characterized by being a convective type of rain (Orellana-Alvear et al., 2017) and ratifies that convective processes can be drivers of the isotopic composition of rain (Kurita, 2013; Nlend et al., 2020; R. Sánchez-Murillo et al., 2016). The coastline located east of South America is the region through which atmospheric humidity enters the continent and coincides with the place where HR_6 was found. Although the SLLJ is responsible for



bringing humidity to certain areas of South America such as the La Plata basin (Angelis & Salio, 2006), the SLLJ also plays an important role in convective systems (Wang & Paegle, 1996) and transports moisture to the Andes (Jones, 2019). This can be observed in Figure 5 when compared with Figure 1 from the study of Montini et al. (2019). Trajectories of the Amazon basin with an origin south of 5°S show a high percentage of black dots (JJA), this is similar to what is shown in Figure 1b in the cited paper in which during this time of year strong winds cross the southern part of the Amazon forest, transporting large amounts of moisture to the study area

The isotopic composition of precipitation whose trajectory crossed the Amazon basin and originated above 5°N was influenced by several factors (Prec_2 , RH_2 , RH_3 , Prec_6 , Temp_i , SRad_1 , SRad_2 , and Press_i) that vary according to the different seasons. In general, the atmospheric humidity present in the Atlantic Ocean is carried by trade winds to the continent and from there it is transported by the Amazon basin where it contributes with large amounts of moisture (Angelis & Salio, 2006; Vera & Douglas, 2006) from the evaporation and transpiration of the Amazon forest (HR_3 , HR_2 , Srad_1 , and Srad_2). This could indicate that convective processes are important, and could be a sign of MCS generated over the rainforest a day or two before the storm reaches the study area. After that, the air masses continue along the eastern edge of the Andes reaching the study site in which the in situ variables (Press_i and Temp_i) intervene as controllers (Kattan, 2019; Le Duy et al., 2018).

Although for $\delta^{18}\text{O}$ the identified controllers were found to explain a large part of the variance, for D-excess clear controllers were not identified. Maybe the lack of drivers could be because most of the trajectories cross the Amazon (the NAMZ and SAMZ regions) which provides high amounts of recycled moisture (high and sustained in D-excess) and the variation is not so marked during their ascension to the study area.



5. CONCLUSIONS

This study reported the isotopic composition of precipitation at high temporal frequency (during rainstorm events) in a páramo basin during the period October 2017-November 2018. The research was carried out to identify the factors (in situ and regional) that control the isotopic composition of precipitation as well as identifying the trajectories followed by the air masses that transport precipitation to the study site. It was found that for the different trajectories that the air masses follow, regional factors are drivers of the isotopic composition of precipitation. In situ factors such as temperature, pressure, and fraction of different precipitation types are also drivers of isotopic composition, indicating that convective processes influence the composition of WSI. It should be noted that for the D-excess the controllers found did not have a very high explanation of the variance as they did with the $\delta^{18}\text{O}$. Also, we determined 4 predominant sources of moisture during the study period: Orinoco Plains, Amazon basin, Mato Grosso Massif, and Pacific coast. These results provide a clearer idea of the factors that influence the WSI of precipitation at a high-resolution scale in the Andean páramo ecosystem. This type of study can help improve climate models and improve paleoclimate reconstructions in the Andes.



6. REFERENCES

- Agudelo, J., Arias, P. A., Vieira, S. C., & Martínez, J. A. (2018). Influence of longer dry seasons in the Southern Amazon on patterns of water vapor transport over northern South America and the Caribbean. *Climate Dynamics*, *0*(0), 0. <https://doi.org/10.1007/s00382-018-4285-1>
- Angelis, C. F., & Salio, P. (2006). *IMPACTS OF THE LOW LEVEL JETS ON THE PRECIPITATION OVER SOUTHERN SOUTH*. 961–966.
- Araguás-Araguás, L., Froehlich, K., & Rozanski, K. (2000). Deuterium and oxygen-18 isotope composition of precipitation and atmospheric moisture. *Hydrological Processes*, *14*(8), 1341–1355. [https://doi.org/10.1002/1099-1085\(20000615\)14:8<1341::AID-HYP983>3.3.CO;2-Q](https://doi.org/10.1002/1099-1085(20000615)14:8<1341::AID-HYP983>3.3.CO;2-Q)
- Arias, P. A., Martínez, J. A., & Vieira, S. C. (2015). Moisture sources to the 2010 – 2012 anomalous wet season in northern South America. *Climate Dynamics*, *45*(9–10), 2861–2884. <https://doi.org/10.1007/s00382-015-2511-7>
- Benjamin, L., Knobel, L. L., Hall, L. F., Cecil, L. D., & Green, J. R. (2004). Development of a Local Meteoric Water Line for Southeastern Idaho, Western Wyoming, and South-Central Montana. *Usgs*, 1–23.
- Ciric, D., Stojanovic, M., Drumond, A., Nieto, R., & Gimeno, L. (2016). Tracking the origin of moisture over the danube river basin using a Lagrangian approach. *Atmosphere*, *7*(12), 1–12. <https://doi.org/10.3390/atmos7120162>
- Córdova, M., Carrillo-Rojas, G., Crespo, P., Wilcox, B., & Céleri, R. (2015). Evaluation of the Penman-Monteith (FAO 56 PM) Method for Calculating Reference Evapotranspiration Using Limited Data. *Mountain Research and Development*, *35*(3), 230–239. <https://doi.org/10.1659/MRD-JOURNAL-D-14-0024.1>
- Craig, H. (1961). Isotopic Variations in Meteoric Waters. *Science*, *133*(3465), 1702–1703. <https://doi.org/10.1126/science.133.3465.1702>



- Dansgaard, W. (1964). Stable isotopes in precipitation. *Tellus*, 16(4), 436–468.
<https://doi.org/10.3402/tellusa.v16i4.8993>
- Dinçer, T., & Payne, B. R. (1971). An environmental isotope study of the south-western Karst region of Turkey. *Journal of Hydrology*, 14(3–4), 233–258.
[https://doi.org/10.1016/0022-1694\(71\)90037-0](https://doi.org/10.1016/0022-1694(71)90037-0)
- Doughty, C. E., & Goulden, M. L. (2008). Seasonal patterns of tropical forest leaf area index and CO₂ exchange. *Journal of Geophysical Research*, 113(June), 1–12. <https://doi.org/10.1029/2007JG000590>
- Draxler, R. R., & Hess, G. D. (1998). An overview of the HYSPLIT_4 modeling system of trajectories, dispersion, and deposition. *Aust. Met. Mag.*, 47(January), 295–308. <https://doi.org/10.1515/eqc-2014-0003>
- Espinoza, J. C., Garreaud, R., Poveda, G., Arias, P. A., Molina-Carpio, J., Masiokas, M., ... Scaff, L. (2020). Hydroclimate of the Andes Part I: Main Climatic Features. *Frontiers in Earth Science*, 8(March), 1–20.
<https://doi.org/10.3389/feart.2020.00064>
- Esquivel-Hernández, G., Mosquera, G. M., Sánchez-Murillo, R., Quesada-Román, A., Birkel, C., Crespo, P., ... Boll, J. (2019). Moisture transport and seasonal variations in the stable isotopic composition of rainfall in Central American and Andean Páramo during El Niño conditions (2015–2016). *Hydrological Processes*, 33(13), 1802–1817. <https://doi.org/10.1002/hyp.13438>
- Froehlich, K., Gibson, J. J., & Aggarwal, P. K. (2002). *Deuterium excess in precipitation and its* The construction of the LMWL will be carried out by regression using the isotopic composition data of $\delta^{18}O$ and δ^2H from the precipitation samples and the adjustment of the LMWL will be assessed using the coefficient. Retrieved from
https://inis.iaea.org/collection/NCLCollectionStore/_Public/34/017/34017972.pdf



Froehlich, Klaus, Kralik, M., Papesch, W., Rank, D., Scheifinger, H., & Stichler, W. (2008). Deuterium excess in precipitation of Alpine regions - Moisture recycling. *Isotopes in Environmental and Health Studies*, 44(1), 61–70. <https://doi.org/10.1080/10256010801887208>

Gastmans, D., Santos, V., Galhardi, J. A., Gromboni, J. F., Batista, L. V., Miotlinski, K., ... Govone, J. S. (2017). Controls over spatial and seasonal variations on isotopic composition of the precipitation along the central and eastern portion of Brazil. *Isotopes in Environmental and Health Studies*, 53(5), 518–538. <https://doi.org/10.1080/10256016.2017.1305376>

Gimeno, L., & Beniston, M. (2013). Grand challenges in atmospheric science. *Frontiers in Earth Science*, 1(October), 1–5. <https://doi.org/10.3389/feart.2013.00001>

Hair Jr, J. F., Hult, G. T. M., Ringle, C., & Sarstedt, M. (2016). *A Primer on Partial Least Squares Structural Equation* (Sage publi).

He, S., Goodkin, N. F., Jackisch, D., Ong, M. R., & Samanta, D. (2018). Continuous real-time analysis of the isotopic composition of precipitation during tropical rain events: Insights into tropical convection. *Hydrological Processes*, 32(11), 1531–1545. <https://doi.org/10.1002/hyp.11520>

Heydarizad, M., Raeisi, E., Sori, R., & Gimeno, L. (2019). An overview of the atmospheric moisture transport effect on stable isotopes ($\delta^{18}\text{O}$, $\delta^2\text{H}$) and D excess contents of precipitation in Iran. *Theoretical and Applied Climatology*. <https://doi.org/10.1007/s00704-019-02798-9>

IAEA. (2014). *IAEA/GNIP precipitation sampling guide*, International Atomic Energy Agency. Vienna, Austria.

Ingraham, N. L. (1998). Isotopic Variations in Precipitation. In *Isotope Tracers in Catchment Hydrology*. <https://doi.org/10.1016/B978-0-444-81546-0.50010-0>



- Jiménez-Sánchez, G., Markowski, P. M., Young, G. S., & Stensrud, D. J. (2020). The Orinoco Low-Level Jet: An Investigation of Its Mechanisms of Formation Using the WRF Model. *Journal of Geophysical Research: Atmospheres*, 125(13), 1–23. <https://doi.org/10.1029/2020JD032810>
- Jones, C. (2019). Recent changes in the South America low-level jet. *Npj Climate and Atmospheric Science*, (May), 1–8. <https://doi.org/10.1038/s41612-019-0077-5>
- Kaseke, K. F., Wang, L., Wanke, H., Tian, C., & Lanning, M. (2018). Precipitation origins and key drivers of precipitation isotope (^{18}O , ^2H , ^{17}O) compositions over Windhoek Running title : Precipitation isotopes over Windhoek. *Journal of Geophysical Research: Atmospheres*, 123(14), 7311–7330. <https://doi.org/10.1029/2018JD028470>
- Kattan, Z. (2019). Factors controlling stable isotopes variability in precipitation in Syria: Statistical analysis approach. *Journal of Earth System Science*, 128(6), 1–25. <https://doi.org/10.1007/s12040-019-1142-5>
- Kendall, C., & McDonnell, J. J. (2012). Isotope tracers in catchment hydrology. In Elsevier (Ed.), *Isotope Tracers in Catchment Hydrology*. <https://doi.org/10.1016/B978-0-444-81546-0.50024-0>
- Kurita, N. (2013). *Water isotopic variability in response to mesoscale convective system*. 118(December 2012), 376–390. <https://doi.org/10.1002/jgrd.50754>
- Lawrence, M. G. (2005). The Relationship between Relative Humidity and the Dewpoint Temperature in Moist Air: A Simple Conversion and Applications. *Bulletin of the American Meteorological Society*, 86(2), 225–233.
- Le Duy, N., Heidbüchel, I., Meyer, H., Merz, B., & Apel, H. (2018). What controls the stable isotope composition of precipitation in the Mekong Delta? A model-based statistical approach. *Earth Syst. Sci*, 225194, 1239–1262. <https://doi.org/10.5194/hess-22-1239-2018>



- Leibundgut, C., Maloszewski, P., & Külls, C. (2009). *Tracers in Hydrology*. John Wiley & Sons.
- Liebming, A., Haberhauer, G., Papesch, W., & Heiss, G. (2006). Correlation of the isotopic composition in precipitation with local conditions in alpine regions. *Journal of Geophysical Research Atmospheres*, 111(5).
<https://doi.org/10.1029/2005JD006258>
- Lin, D., Foster, D. P., & Ungar, L. H. (2011). VIF regression: A fast regression algorithm for large data. *Journal of the American Statistical Association*, 106(493), 232–247. <https://doi.org/10.1198/jasa.2011.tm10113>
- McDonnell, J. J., Bonell, M., Stewart, M. K., & Pearce, A. J. (1990). Deuterium Variations in Storm Rainfall : Implications for Stream Hydrograph Separation. *Water Resources Research*, 26(3), 455–458.
<https://doi.org/10.1029/WR026i003p00455>
- Montini L., T., Jones, C., & Carvalho, L. (2019). The South American Low-Level Jet: A New Climatology, Variability, and Changes. *Journal of Geophysical Research: Atmospheres*, 1. <https://doi.org/10.1029/2018JD029634>
- Montini, T. L., Jones, C., & Carvalho, L. M. V. (2019). The South American Low-Level Jet: A New Climatology, Variability, and Changes. *Journal of Geophysical Research: Atmospheres*, 124(3), 1200–1218.
<https://doi.org/10.1029/2018JD029634>
- Mook, W., & Rozanski, K. (2000). Environmental isotopes in the hydrological cycle. *IAEA Publish*, 39.
- Mosquera, G. M., Céleri, R., Lazo, P. X., Vaché, K. B., Perakis, S. S., & Crespo, P. (2016). Combined use of isotopic and hydrometric data to conceptualize ecohydrological processes in a high-elevation tropical ecosystem. *Hydrological Processes*, 30(17), 2930–2947. <https://doi.org/10.1002/hyp.10927>



- Mosquera, G. M., Lazo, P. X., Céleri, R., Wilcox, B. P., & Crespo, P. (2015). Runoff from tropical alpine grasslands increases with areal extent of wetlands. *Catena*, *125*, 120–128. <https://doi.org/10.1016/j.catena.2014.10.010>
- Mosquera, G. M., Segura, C., Vaché, K. B., Windhorst, D., Breuer, L., & Crespo, P. (2016). Insights into the water mean transit time in a high-elevation tropical ecosystem. *Hydrology and Earth System Sciences*, *20*(7), 2987–3004. <https://doi.org/10.5194/hess-20-2987-2016>
- Muñoz, P., Céleri, R., & Feyen, J. (2016). *Effect of the Resolution of Tipping-Bucket Rain Gauge and Calculation Method on Rainfall Intensities in an Andean Mountain Gradient*. (1992). <https://doi.org/10.3390/w8110534>
- Nlend, B., Celle-Jeanton, H., Risi, C., Pohl, B., Huneau, F., Ngo Boum-Nkot, S., ... Ketchemen-Tandia, B. (2020). Identification of processes that control the stable isotope composition of rainwater in the humid tropical West-Central Africa. *Journal of Hydrology*, *584*(February), 124650. <https://doi.org/10.1016/j.jhydrol.2020.124650>
- Noone, D. (2012). Pairing measurements of the water vapor isotope ratio with humidity to deduce atmospheric moistening and dehydration in the tropical midtroposphere. *Journal of Climate*, *25*(13), 4476–4494. <https://doi.org/10.1175/JCLI-D-11-00582.1>
- Orellana-Alvear, J., Céleri, R., Rollenbeck, R., & Bendix, J. (2017). Analysis of rain types and their Z-R relationships at different locations in the high andes of southern Ecuador. *Journal of Applied Meteorology and Climatology*, *56*(11), 3065–3080. <https://doi.org/10.1175/JAMC-D-17-0009.1>
- Padrón, R. S., Wilcox, B. P., Crespo, P., & Céleri, R. (2015). Rainfall in the Andean Páramo: New Insights from High-Resolution Monitoring in Southern Ecuador. *Journal of Hydrometeorology*, *16*(3), 985–996. <https://doi.org/10.1175/JHM-D-14-0135.1>



- Pang, Z., Kong, Y., Froehlich, K., Huang, T., Yuan, L., Li, Z., & Wang, F. (2011). Processes affecting isotopes in precipitation of an arid region. *Tellus, Series B: Chemical and Physical Meteorology*, 63(3), 352–359. <https://doi.org/10.1111/j.1600-0889.2011.00532.x>
- Penna, D., Stenni, B., Šanda, M., Wrede, S., Bogaard, T. A., Michelini, M., ... Wassenaar, L. I. (2012). Technical note: Evaluation of between-sample memory effects in the analysis of $\delta^2\text{H}$ and $\delta^{18}\text{O}$ of water samples measured by laser spectrometers. *Hydrology and Earth System Sciences*, 16(10), 3925–3933. <https://doi.org/10.5194/hess-16-3925-2012>
- Picarro. (2010). ChemCorrect™ - Solving the Problem of Chemical Contaminants in H_2O Stable Isotope Research. *White Paper*, 2–4.
- Poveda, G., Jaramillo, L., & Vallejo, L. F. (2014). *Seasonal precipitation patterns along pathways of South American low-level jets and aerial rivers* *Germ.* 50(3), 98–118. <https://doi.org/10.1002/2013WR014087>
- Putman, A. L., Fiorella, R. P., Bowen, G. J., & Cai, Z. (2019). A Global Perspective on Local Meteoric Water Lines: Meta-analytic Insight Into Fundamental Controls and Practical Constraints. *Water Resources Research*. <https://doi.org/10.1029/2019wr025181>
- Rindsberger, M., M. Magaritz, I. C., & Gilad, D. (1983). The relation between air mass trajectories and the water isotope composition of rain in the Mediterranean Sea area. *Geophysical Research Letters*, 10(1), 43–46. <https://doi.org/10.1029/GL010i001p00043>
- Rolph, G., Stein, A., & Stunder, B. (2017). Real-time Environmental Applications and Display sYstem: READY. *Environmental Modelling and Software*, 95, 210–228. <https://doi.org/10.1016/j.envsoft.2017.06.025>
- Rozanski, K., & Araguas, L. A. (1995). Spatial and temporal variability of stable isotope composition of precipitation over the South American continent.



Bulletin de l'Institut Francais d'etudes Andines, 24(3), 379–390. Retrieved from papers3://publication/uuid/0DBCD095-3531-4286-B818-8CA24DA75DB6

- Rozanski, Kazimierz, Araguás-Araguás, L., & Gonfiantini, R. (1993). Isotopic Patterns in Modern Global Precipitation. *International Atomic Energy Agency*. <https://doi.org/10.1029/GM078p0001>
- Ruiz-Vásquez, M., Arias, P. A., Martínez, J. A., & Espinoza, J. C. (2020). Effects of Amazon basin deforestation on regional atmospheric circulation and water vapor transport towards tropical South America. *Climate Dynamics*, (0123456789). <https://doi.org/https://doi.org/10.1007/s00382-020-05223-4>
- Sakamoto, M. S. (2011). Moisture Sources and Life Cycle of Convective Systems over Western Colombia. *Advances in Meteorology*, 2011. <https://doi.org/10.1155/2011/890759>
- Salati, E., Dall'Olio, A., Matsui, E., & Gat, J. R. (1979). Recycling of water in the Amazon Basin: An isotopic study. *Water Resources Research*, 15(5), 1250–1258. <https://doi.org/10.1029/WR015i005p01250>
- Sánchez-Murillo, R., Birkel, C., Welsh, K., Esquivel-Hernández, G., Corrales-Salazar, J., Boll, J., ... Araguás-Araguás, L. J. (2016). Key drivers controlling stable isotope variations in daily precipitation of Costa Rica: Caribbean Sea versus Eastern Pacific Ocean moisture sources. *Quaternary Science Reviews*, 131, 250–261. <https://doi.org/10.1016/j.quascirev.2015.08.028>
- Sánchez-Murillo, Ricardo, Durán-Quesada, A. M., Birkel, C., Esquivel-Hernández, G., & Boll, J. (2017). Tropical precipitation anomalies and d-excess evolution during El Niño 2014-16. *Hydrological Processes*, 31(4), 956–967. <https://doi.org/10.1002/hyp.11088>
- Sloat, L. L., Gerber, J. S., Samberg, L. H., Smith, W. K., Herrero, M., Ferreira, L. G., ... West, P. C. (2018). Increasing importance of precipitation variability on global livestock grazing lands. *Nature Climate Change*, 8(3), 214–218.



<https://doi.org/10.1038/s41558-018-0081-5>

Stein, A. F., Draxler, R. R., Rolph, G. D., Stunder, B. J. B., Cohen, M. D., & Ngan, F. (2015). Noaa's hysplit atmospheric transport and dispersion modeling system. *Bulletin of the American Meteorological Society*, 96(12), 2059–2077. <https://doi.org/10.1175/BAMS-D-14-00110.1>

Su, L., Yuan, Z., Fung, J. C. H., & Lau, A. K. H. (2015). A comparison of HYSPLIT backward trajectories generated from two GDAS datasets. *Science of the Total Environment*, 506–507, 527–537. <https://doi.org/10.1016/j.scitotenv.2014.11.072>

Thibeault, J., Seth, A., & Wang, G. (2012). Mechanisms of summertime precipitation variability in the bolivian altiplano: Present and future. *International Journal of Climatology*, 32(13), 2033–2041. <https://doi.org/10.1002/joc.2424>

Thies Clima. (2007). *Instructions for use. Laser Precipitation Monitor 5.4110.xx.x00 V2.2xSTD*. 1–58.

Van Der Ent, R. J., & Tuinenburg, O. A. (2017). The residence time of water in the atmosphere revisited. *Hydrology and Earth System Sciences*, 21(2), 779–790. <https://doi.org/10.5194/hess-21-779-2017>

Vera, C., & Douglas, M. W. (2006). *The South American Low-Level Jet Experiment*. (May 2014). <https://doi.org/10.1175/BAMS-87-1-63>

Wang, M., & Paegle, J. (1996). Impact of analysis uncertainty upon regional atmospheric moisture flux. *Journal of Geophysical Research*, 101, 7291–7303.

Windhorst, D., Waltz, T., Timbe, E., Frede, H. G., & Breuer, L. (2013). Impact of elevation and weather patterns on the isotopic composition of precipitation in a tropical montane rainforest. *Hydrology and Earth System Sciences*, 17(1), 409–419. <https://doi.org/10.5194/hess-17-409-2013>

7. SUPPLEMENTARY MATERIAL

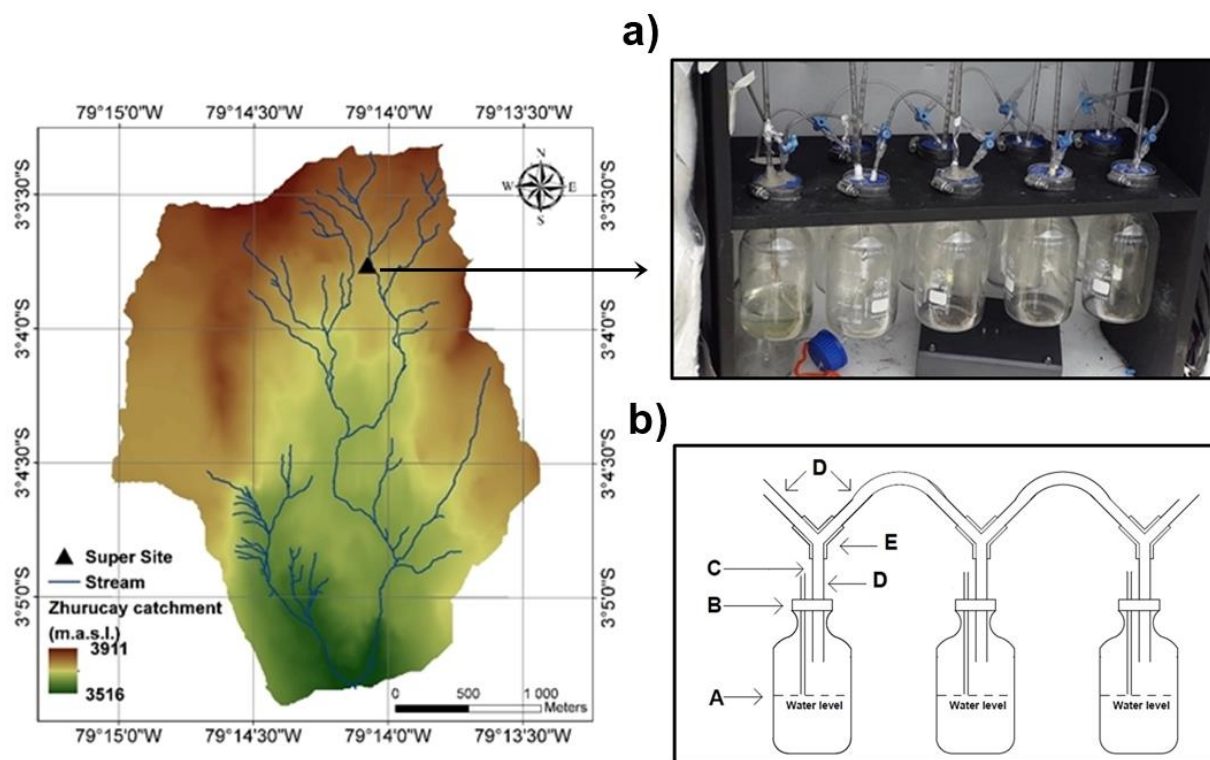


Figure A1. Location of the hand-made sequential rainfall sampler. a) Hand-made sequential rainfall sampler located in the study area. b) Schematic representation (A-Water bottle, B-Stopper, C-Atmospheric pressure tube, D-Water tube and E-Y connector).

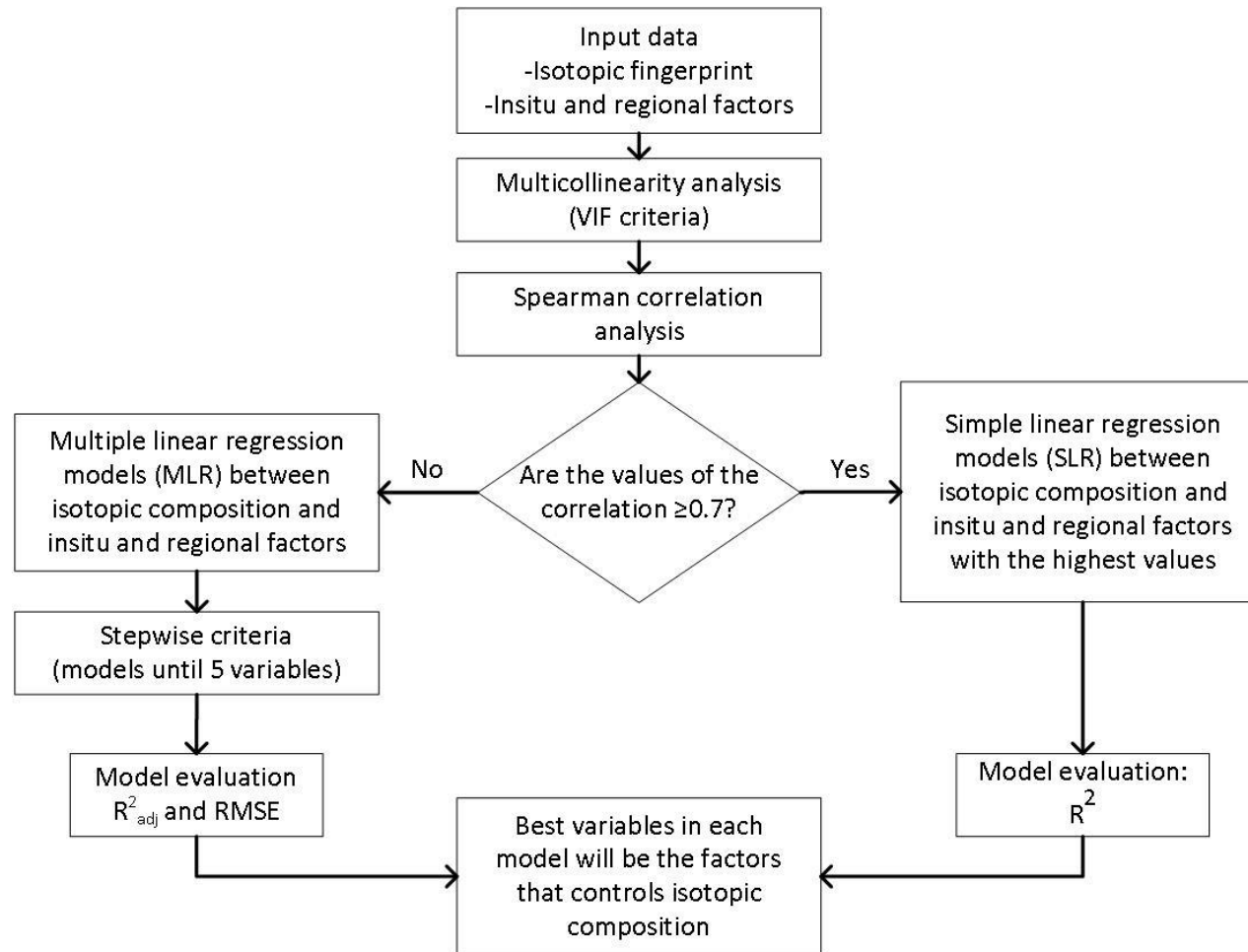


Figure A2. Methodology used in the study to determinate the factors that controls the isotopic composition in precipitation in the study site.

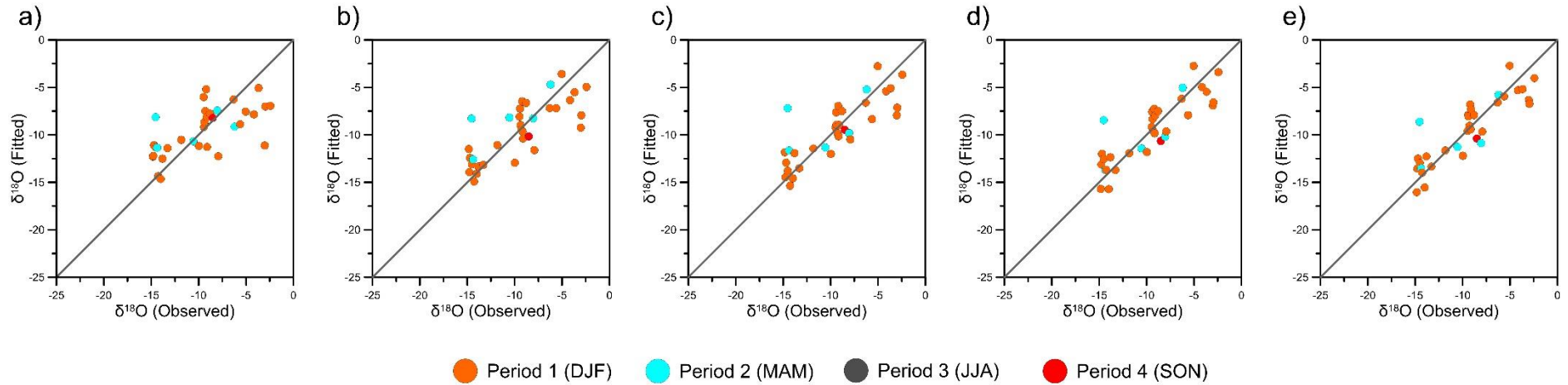


Figure A3. The x-y plot of the $\delta^{18}\text{O}$ signal (observed against simulated) of the precipitation samples whose trajectory crosses the Orinoco plains during the full study period using MLR with different number of variables. a) MLR using 1 variable, b) MLR using 2 variables, c) MLR using 3 variables, d) MLR using 4 variables and e) MLR using 5 variables.

Table A1. Results of the MRLs of the $\delta^{18}\text{O}$ signal from the precipitation samples whose trajectory crosses the Orinoco plains during the full study period using 1 until 5 variables.

Isotopic composition	Model	Variables	R ²	R ² _{aj}	AIC	RMSE	pVal	n
$\delta^{18}\text{O}$	M1	Temp _i	0.407	0.388	172.091	2.9969	6.44E-05	33
	M2	Temp _i , Prec ₅	0.601	0.574	161.061	2.4600	1.05E-06	
	M3	Temp _i , Prec ₅ , M+H+VH	0.667	0.633	157.061	2.2462	4.34E-07	
	M4	Temp _i , Prec ₅ , M+H+VH, Alt ₁	0.738	0.701	151.134	1.9920	8.07E-08	
	M5	Temp _i , Prec ₅ , M+H+VH, Alt ₁ , Alt ₅	0.756	0.711	150.744	1.9212	1.52E-07	

Note. R² = R-squared, R²_{aj} = Adjusted R-squared, AIC = Akaike Information Criterion, RMSE = Root Mean Square Error, pVal = p-value, n = number of samples used for the MLRs

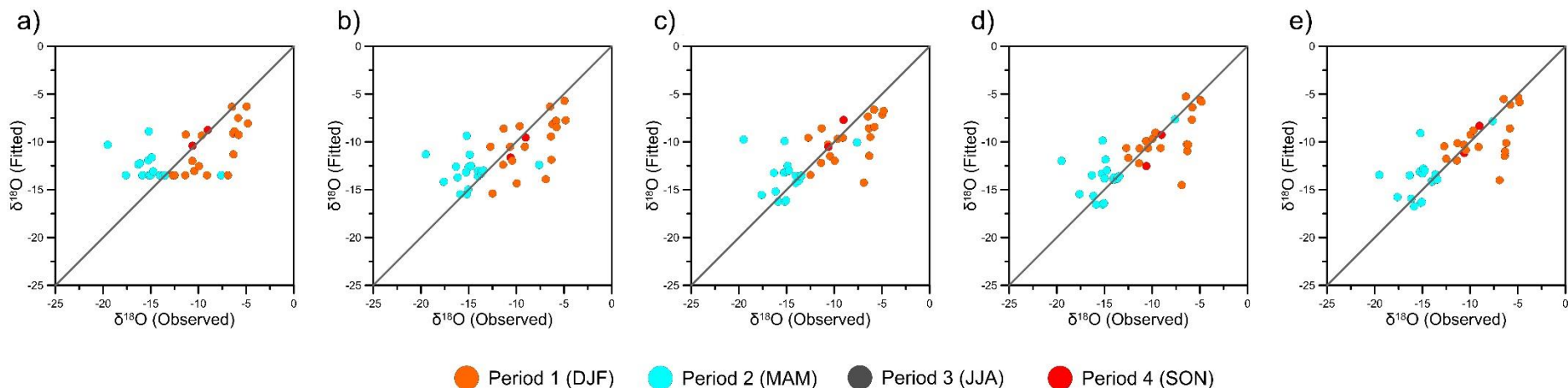


Figure A4. The x-y plot of the $\delta^{18}\text{O}$ signal (observed against simulated) of the precipitation samples whose trajectory crosses the Pacific coast during the full study period using MLR with different number of variables. a) MLR using 1 variable, b) MLR using 2 variables, c) MLR using 3 variables, d) MLR using 4 variables and e) MLR using 5 variables.

Table A2. Results of the MRLs of the $\delta^{18}\text{O}$ signal from the precipitation samples whose trajectory crosses the Pacific coast during the full study period using 1 until 5 variables.

Isotopic composition	Model	Variables	R ²	R ² _{aj}	AIC	RMSE	pVal	n
$\delta^{18}\text{O}$	M1	M+H+VH	0.329	0.310	203.371	3.2480	1.67E-04	38
	M2	M+H+VH, Prec ₁	0.419	0.386	199.909	3.0228	7.50E-05	
	M3	M+H+VH, Prec ₁ , HR ₈	0.494	0.449	196.673	2.8215	3.24E-05	
	M4	M+H+VH, Prec ₁ , HR ₈ , HR ₆	0.581	0.530	191.511	2.5678	6.27E-06	
	M5	M+H+VH, Prec ₁ , HR ₈ , HR ₆ , WindVel _i	0.599	0.537	191.790	2.5103	1.17E-05	

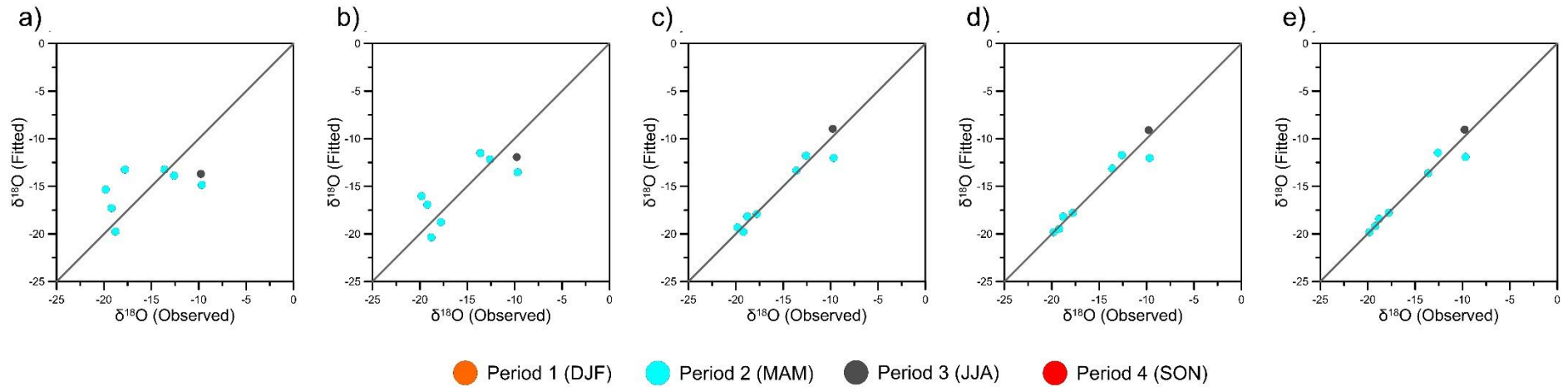


Figure A5. The x-y plot of the $\delta^{18}\text{O}$ signal (observed against simulated) of the precipitation samples whose trajectory crosses the Mato Grosso Massif during the full study period using MLR with different number of variables. a) MLR using 1 variable, b) MLR using 2 variables, c) MLR using 3 variables, d) MLR using 4 variables and e) MLR using 5 variables.

Table A3. Results of the MRLs of the $\delta^{18}\text{O}$ signal from the precipitation samples whose trajectory crosses the Mato Grosso Massif during the full study period using 1 until 5 variables.

Isotopic composition	Model	Variables	R^2	R^2_{aj}	AIC	RMSE	pVal	n
$\delta^{18}\text{O}$	M1	HR	0.293	0.175	48.002	3.3407	1.66E-01	8
	M2	HR _i , Prec ₄	0.627	0.478	44.871	2.4242	8.47E-02	
	M3	HR _i , Prec ₄ , SRad _i	0.938	0.891	32.538	0.9897	7.08E-03	
	M4	HR _i , Prec ₄ , SRad _i , Prec ₅	0.941	0.863	34.108	0.9635	3.44E-02	
	M5	HR _i , Prec ₄ , SRad _i , Prec ₅ , Prec ₇	0.945	0.806	35.621	0.9346	1.33E-01	

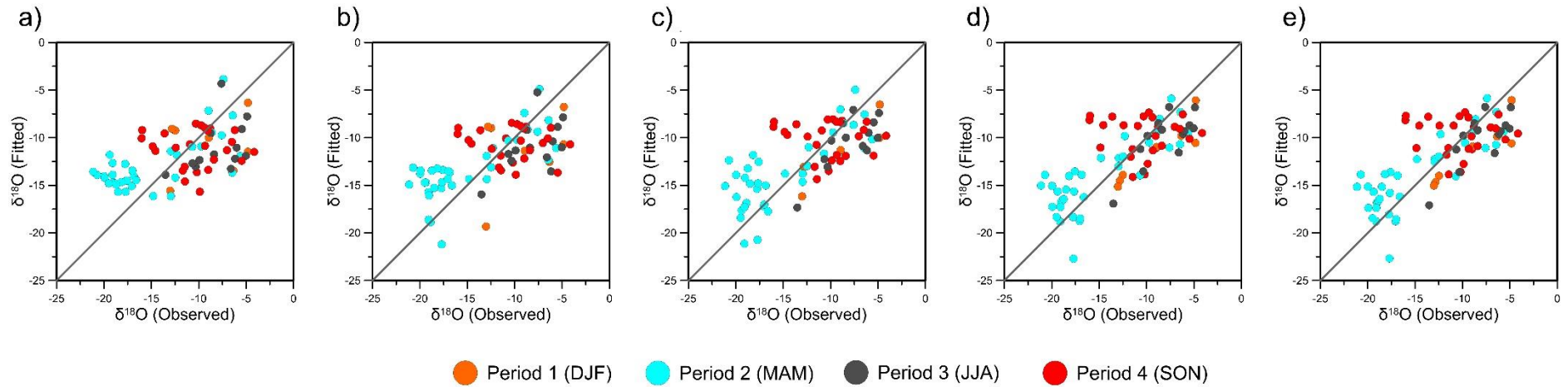


Figure A6. The x-y plot of the $\delta^{18}\text{O}$ signal (observed against simulated) of the precipitation samples whose trajectory crosses the Amazon basin and whose origin are between 5°N and 5°S for the full study period using MLR with different number of variables. a) MLR using 1 variable, b) MLR using 2 variables, c) MLR using 3 variables, d) MLR using 4 variables and e) MLR using 5 variables.

Table A4. Results of the MRLs of the $\delta^{18}\text{O}$ signal from the precipitation samples whose trajectory crosses Amazon basin and whose origin are between 5°N and 5°S during the full study period using 1 until 5 variables.

Isotopic composition	Model	Variables	R^2	R^2_{aj}	AIC	RMSE	pVal	n
$\delta^{18}\text{O}$	M1	MD ₄	0.299	0.290	457.153	4.058	1.54E-07	80
	M2	MD ₄ , Prec ₇	0.390	0.374	448.046	3.786	5.49E-09	
	M3	MD ₄ , Prec ₇ , Prec ₆	0.496	0.476	434.737	3.441	2.45E-11	
	M4	MD ₄ , Prec ₇ , Prec ₆ , Prec ₃	0.562	0.538	425.569	3.209	8.09E-13	
	M5	MD ₄ , Prec ₇ , Prec ₆ , Prec ₃ , Prec ₅	0.562	0.533	427.465	3.207	4.08E-12	

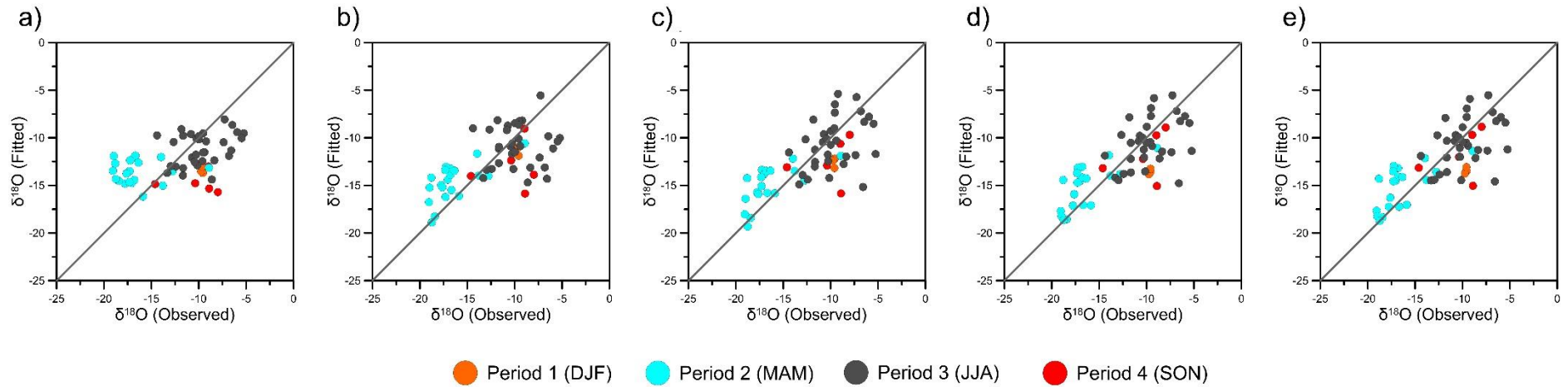


Figure A7. The x-y plot of the $\delta^{18}\text{O}$ signal (observed against simulated) of the precipitation samples whose trajectory crosses the Amazon basin and whose origin are under $d 5^{\circ}\text{S}$ for the full study period using MLR with different number of variables. a) MLR using 1 variable, b) MLR using 2 variables, c) MLR using 3 variables, d) MLR using 4 variables and e) MLR using 5 variables.

Table A5. Results of the MRLs of the $\delta^{18}\text{O}$ signal from the precipitation samples whose trajectory crosses the Amazon basin and whose origin are under $d 5^{\circ}\text{S}$ during the full study period using 1 until 5 variables.

Isotopic composition	Model	Variables	R^2	R^2_{aj}	AIC	RMSE	pVal	n
$\delta^{18}\text{O}$	M1	Temp _i	0.213	0.199	352.438	3.515	3.47E-04	60
	M2	Temp _i , Press _i	0.378	0.356	338.464	3.134	8.79E-07	
	M3	Temp _i , Press _i , HR ₆	0.485	0.457	328.421	2.857	1.74E-08	
	M4	Temp _i , Press _i , HR ₆ , H+VH	0.534	0.500	327.392	2.716	2.15E-08	
	M5	Temp _i , Press _i , HR ₆ , H+VH, Prec4	0.536	0.493	329.163	2.711	8.18E-08	

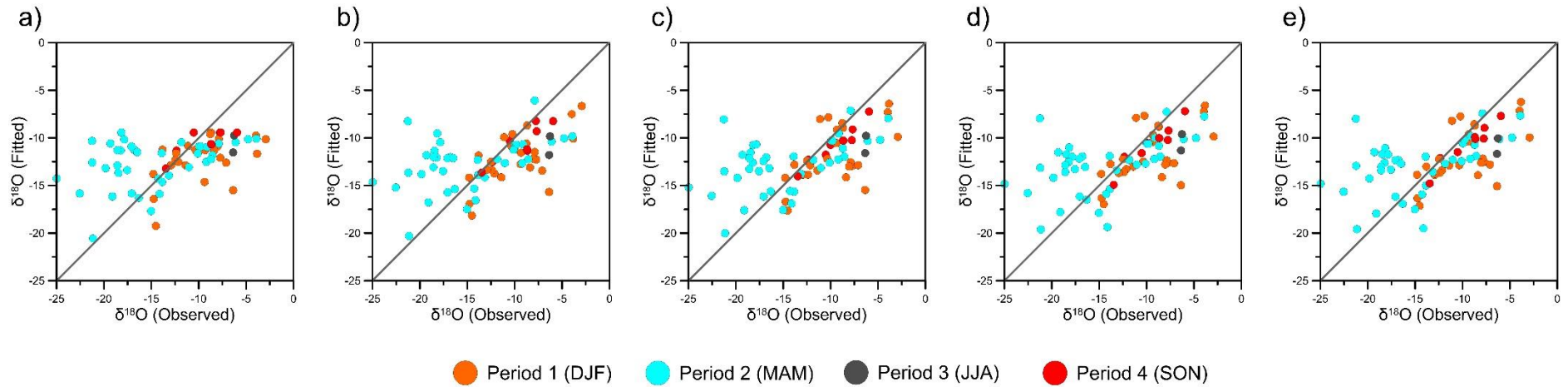


Figure A8. The x-y plot of the $\delta^{18}\text{O}$ signal (observed against simulated) of the precipitation samples whose trajectory crosses the Amazon basin and whose origin are above 5°N for the full study period using MLR with different number of variables. a) MLR using 1 variable, b) MLR using 2 variables, c) MLR using 3 variables, d) MLR using 4 variables and e) MLR using 5 variables.

Table A6. Results of the MRLs of the $\delta^{18}\text{O}$ signal from the precipitation samples whose trajectory crosses the Amazon basin and whose origin are above 5°N during the full study period using 1 until 5 variables.

Isotopic composition	Model	Variables	R^2	R^2_{aj}	AIC	RMSE	pVal	n
$\delta^{18}\text{O}$	M1	Prec ₂	0.217	0.207	447.650	4.422	2.21E-05	76
	M2	Prec ₂ , HR ₂	0.268	0.248	444.503	4.275	1.11E-05	
	M3	Prec ₂ , HR ₂ , HR ₃	0.312	0.283	441.884	4.147	5.70E-06	
	M4	Prec ₂ , HR ₂ , HR ₃ , Prec ₆	0.319	0.281	443.023	4.124	1.44E-05	
	M5	Prec ₂ , HR ₂ , HR ₃ , Prec ₆ , Temp _i	0.321	0.273	444.830	4.118	4.23E-05	

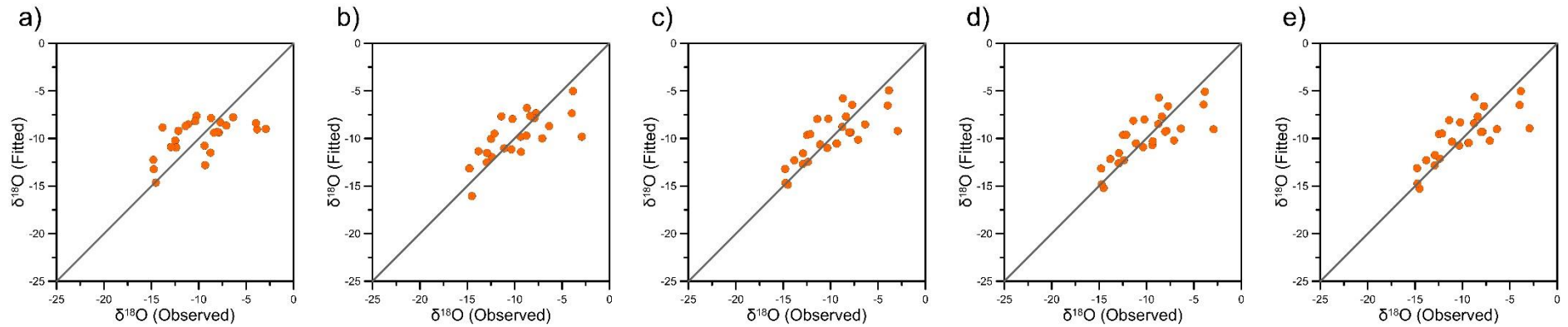


Figure A9. The x-y plot of the $\delta^{18}\text{O}$ signal (observed against simulated) of the precipitation samples from the period 1 (December-February) and whose trajectory crosses the Amazon basin and whose origin are above 5°N using MLR with different number of variables. a) MLR using 1 variable, b) MLR using 2 variables, c) MLR using 3 variables, d) MLR using 4 variables and e) MLR using 5 variables.

Table A7. Results of the MRLs of the $\delta^{18}\text{O}$ signal from the precipitation samples from the period 1 (December-February) and whose trajectory crosses the Amazon basin and whose origin are above 5°N using 1 until 5 variables.

Isotopic composition	Model	Variables	R^2	R^2_{aj}	AIC	RMSE	pVal	n
$\delta^{18}\text{O}$	M1	SRad ₁	0.299	0.269	132.644	2.764	3.87E-03	26
	M2	SRad ₁ , Temp _i	0.531	0.490	124.176	2.260	1.65E-04	
	M3	SRad ₁ , Temp _i , SRad ₂	0.584	0.527	123.073	2.129	1.97E-04	
	M4	SRad ₁ , Temp _i , SRad ₂ , Prec ₂	0.587	0.508	124.906	2.122	6.72E-04	
	M5	SRad ₁ , Temp _i , SRad ₂ , Prec ₂ , Prec ₁	0.588	0.485	126.805	2.118	1.97E-03	

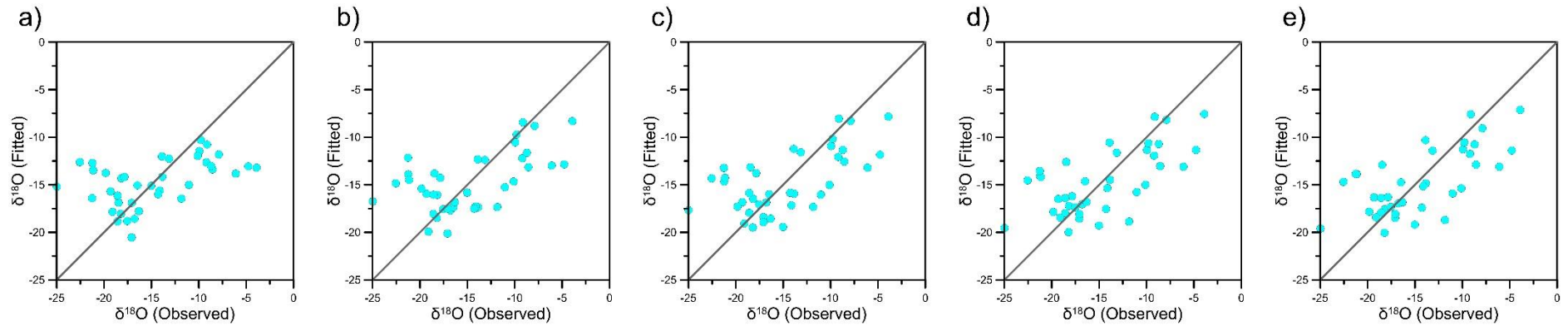


Figure A10. The x-y plot of the $\delta^{18}\text{O}$ signal (observed against simulated) of the precipitation samples from the period 2 (March-May) and whose trajectory crosses the Amazon basin and whose origin are above 5°N using MLR with different number of variables. a) MLR using 1 variable, b) MLR using 2 variables, c) MLR using 3 variables, d) MLR using 4 variables and e) MLR using 5 variables..

Table A8. Results of the MRLs of the $\delta^{18}\text{O}$ signal from the precipitation samples from the period 2 (March-May) and whose trajectory crosses the Amazon basin and whose origin are above 5°N using 1 until 5 variables.

Isotopic composition	Model	Variables	R^2	R^2_{aj}	AIC	RMSE	pVal	n
$\delta^{18}\text{O}$	M1	Press	0.442	0.424	234.399	3.633	2.11E-03	34
	M2	Press _i , HR ₃	0.544	0.515	229.810	3.281	4.53E-04	
	M3	Press _i , HR ₃ , SRad ₈	0.554	0.509	229.180	3.228	5.41E-04	
	M4	Press _i , HR ₃ , SRad ₈ , SRad ₇	0.559	0.498	229.249	3.195	7.75E-04	
	M5	Press _i , HR ₃ , SRad ₈ , SRad ₇ , HR ₂	0.562	0.484	231.109	3.183	2.04E-03	

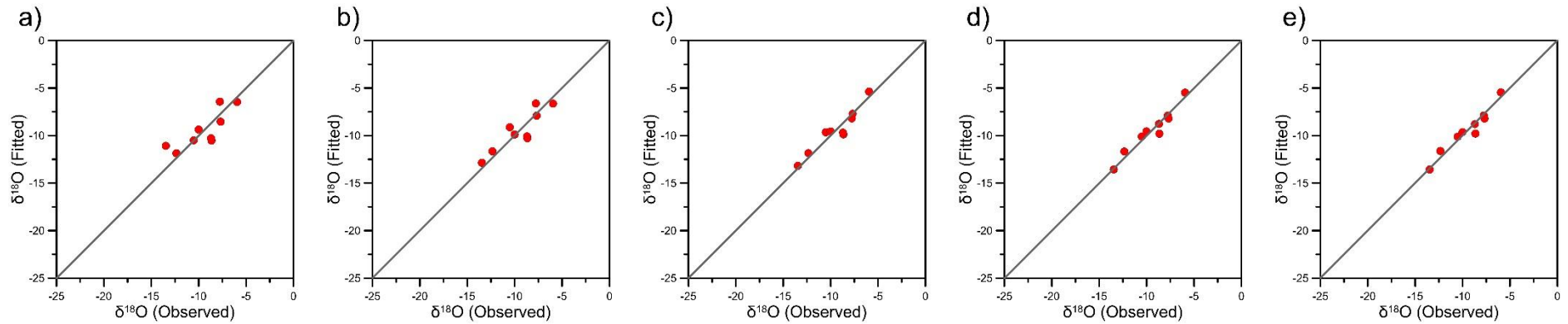


Figure A11. The x-y plot of the $\delta^{18}\text{O}$ signal (observed against simulated) of the precipitation samples from the period 4 (September-November) and whose trajectory crosses the Amazon basin and whose origin are above 5°N using MLR with different number of variables. a) MLR using 1 variable, b) MLR using 2 variables, c) MLR using 3 variables, d) MLR using 4 variables and e) MLR using 5 variables.

Table A9. Results of the MRLs of the $\delta^{18}\text{O}$ signal from the precipitation samples from the period 4 (September-November) and whose trajectory crosses the Amazon basin and whose origin are above 5°N using 1 until 5 variables.

Isotopic composition	Model	Variables	R^2	R^2_{aj}	AIC	RMSE	pVal	n
$\delta^{18}\text{O}$	M1	HR ₂	0.666	0.618	36.224	1.297	7.29E-03	9
	M2	HR ₂ , Prec ₂	0.797	0.729	33.752	1.012	8.38E-03	
	M3	HR ₂ , Prec ₂ , MD ₃	0.906	0.850	28.801	0.688	5.30E-03	
	M4	HR ₂ , Prec ₂ , MD ₃ , Press _i	0.941	0.882	26.655	0.546	1.01E-02	
	M5	HR ₂ , Prec ₂ , MD ₃ , Press _i , SRad ₈	0.941	0.843	28.617	0.545	4.60E-02	

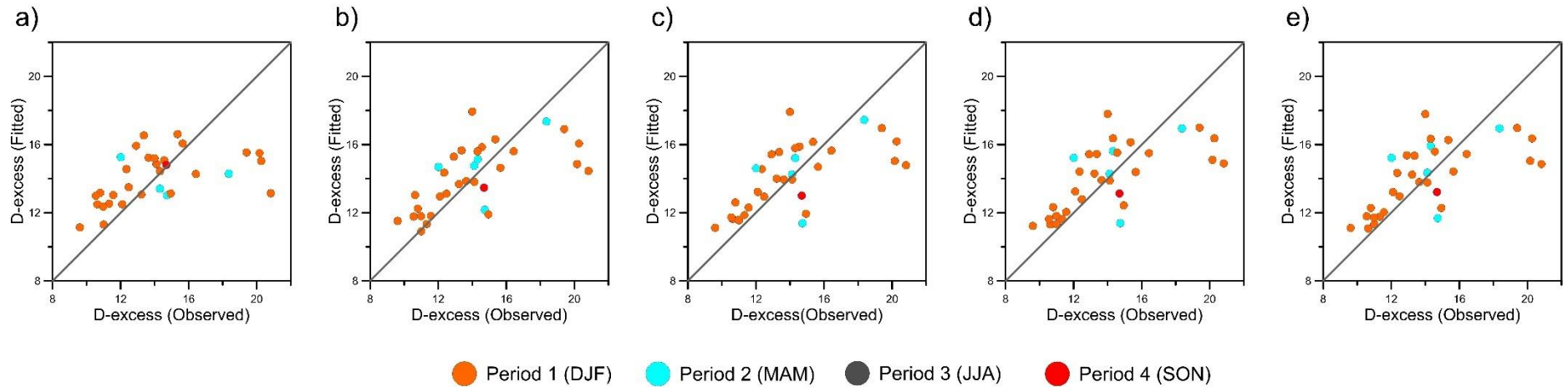


Figure A12. The x-y plot of the D-excess signal (observed against simulated) of the precipitation samples whose trajectory crosses the Orinoco plains during the full study period using MLR with different number of variables. a) MLR using 1 variable, b) MLR using 2 variables, c) MLR using 3 variables, d) MLR using 4 variables and e) MLR using 5 variables.

Table A10. Results of the MRLs of the D-excess signal from the precipitation samples whose trajectory crosses the Orinoco plains during the full study period using 1 until 5 variables.

Isotopic composition	Model	Variables	R ²	R ² _{aj}	AIC	RMSE	pVal	n
D-excess	M1	Temp _i	0.234	0.210	161.810	2.565	4.30E-03	33
	M2	Temp _i , HR ₁	0.398	0.358	155.896	2.275	4.98E-04	
	M3	Temp _i , HR ₁ , Prec ₅	0.415	0.354	156.939	2.242	1.25E-03	
	M4	Temp _i , HR ₁ , Prec ₅ , M+H+VH	0.423	0.340	158.488	2.227	3.15E-03	
	M5	Temp _i , HR ₁ , Prec ₅ , M+H+VH, Prec ₄	0.424	0.318	160.398	2.224	7.80E-03	

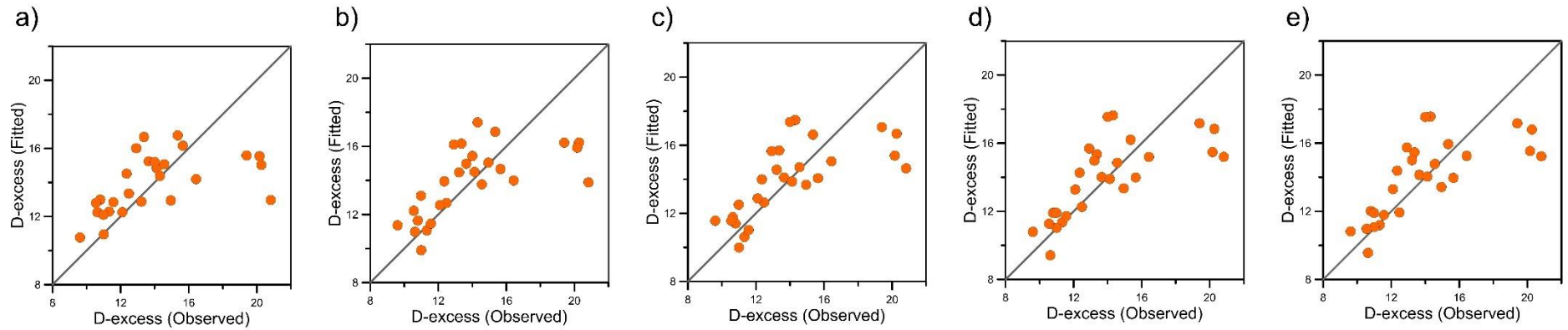


Figure A13. The x-y plot of the D-excess signal (observed against simulated) of the precipitation samples from DJF and whose trajectory crosses the Orinoco plains using MLR with different number of variables. a) MLR using 1 variable, b) MLR using 2 variables, c) MLR using 3 variables, d) MLR using 4 variables and e) MLR using 5 variables.

Table A11. Results of the MRLs of the D-excess signal from the precipitation samples from the period 1 DJF and whose trajectory crosses the Orinoco plains using 1 until 5 variables.

Isotopic composition	Model	Variables	R ²	R ² _{aj}	AIC	RMSE	pVal	n
D-excess	M1	Temp _i	0.288	0.260	134.555	2.616	3.90E-03	27
	M2	Temp _i , HR ₁	0.419	0.370	131.086	2.364	1.49E-03	
	M3	Temp _i , HR ₁ , M+H+VH	0.470	0.401	130.570	2.257	1.89E-03	
	M4	Temp _i , HR ₁ , M+H+VH, Prec ₅	0.511	0.422	130.440	2.169	2.56E-03	
	M5	Temp _i , HR ₁ , M+H+VH, Prec ₅ , Prec ₄	0.512	0.396	132.351	2.166	6.68E-03	

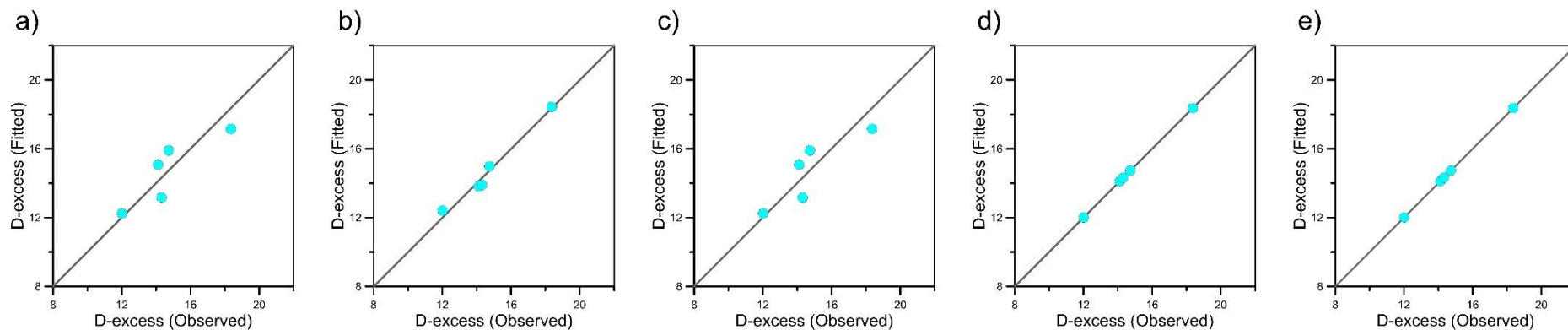


Figure A14. The x-y plot of the D-excess signal (observed against simulated) of the precipitation samples from MAM and whose trajectory crosses the Orinoco plains using MLR with different number of variables. a) MLR using 1 variable, b) MLR using 2 variables, c) MLR using 3 variables, d) MLR using 4 variables and e) MLR using 5 variables.

Table A12. Results of the MRLs of the D-excess signal from the precipitation samples from MAM and whose trajectory crosses the Orinoco plains using 1 until 5 variables.

Isotopic composition	Model	Variables	R ²	R ² _{aj}	AIC	RMSE	pVal	n
D-excess	M1	HR ₁	0.759	0.678	20.284	1.010	0.054	5
	M2	HR ₁ , HR ₈	0.977	0.953	10.611	0.314	0.023	
	M3	HR ₁ , HR ₈ , Alt ₇	0.993	0.973	6.327	0.168	0.104	
	M4	HR ₁ , HR ₈ , Alt ₇ , Temp _i	1.000	-	-	-	-	
	M5	HR ₁ , HR ₈ , Alt ₇ , Temp _i , Press _i	1.000	-	-	-	-	

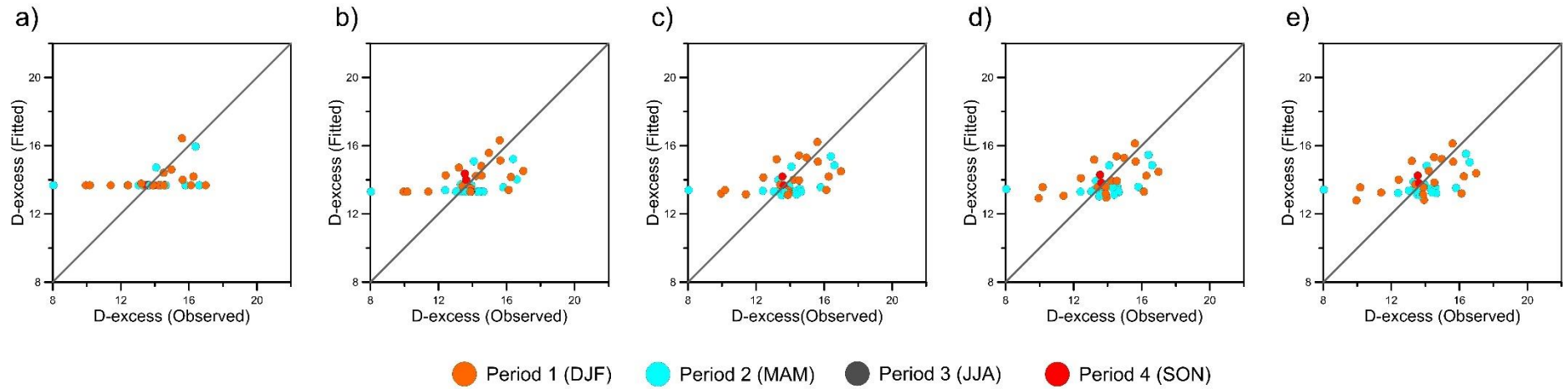


Figure A15. The x-y plot of the D-excess signal (observed against simulated) of the precipitation samples whose trajectory crosses the Pacific coast during the full study period using MLR with different number of variables. a) MLR using 1 variable, b) MLR using 2 variables, c) MLR using 3 variables, d) MLR using 4 variables and e) MLR using 5 variables.

Table A13. Results of the MRLs of the D-excess signal from the precipitation samples whose trajectory crosses the Pacific coast during the full study period using 1 until 5 variables.

Isotopic composition	Model	Variables	R ²	R ² _{aj}	AIC	RMSE	pVal	n
D-excess	M1	Prec ₈	0.110	0.085	154.455	1.706	4.23E-02	38
	M2	Prec ₈ , M+H+VH	0.180	0.133	153.318	1.637	3.09E-02	
	M3	Prec ₈ , M+H+VH, WindVel _i	0.197	0.126	154.517	1.620	5.56E-02	
	M4	Prec ₈ , M+H+VH, WindVel _i , Prec ₁	0.201	0.104	156.349	1.617	1.07E-01	
	M5	Prec ₈ , M+H+VH, WindVel _i , Prec ₁ , Prec ₃	0.206	0.082	158.110	1.612	1.73E-01	

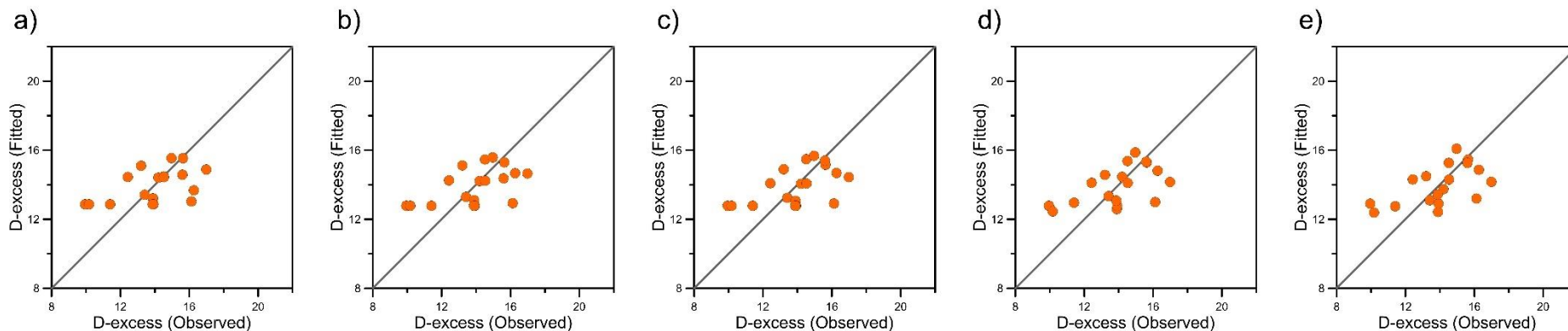


Figure A 16. The x-y plot of the D-excess signal (observed against simulated) of the precipitation samples from DJF and whose trajectory crosses the Pacific coast using MLR with different number of variables. a) MLR using 1 variable, b) MLR using 2 variables, c) MLR using 3 variables, d) MLR using 4 variables and e) MLR using 5 variables.

Table A14. Results of the MRLs of the D-excess signal from the precipitation samples from DJF and whose trajectory crosses the Pacific coast using 1 until 5 variables.

Isotopic composition	Model	Variables	R ²	R ² _{aj}	AIC	RMSE	pVal	n
D-excess	M1	M+H+VH	0.244	0.197	75.596	1.672	3.72E-02	18
	M2	M+H+VH, Prec ₇	0.278	0.182	76.763	1.634	8.68E-02	
	M3	M+H+VH, Prec ₇ , Prec ₈	0.297	0.147	78.279	1.612	1.64E-01	
	M4	M+H+VH, Prec ₇ , Prec ₈ , HR ₈	0.311	0.099	79.919	1.596	2.68E-01	
	M5	M+H+VH, Prec ₇ , Prec ₈ , HR ₈ , Prec ₃	0.326	0.045	81.522	1.579	3.82E-01	

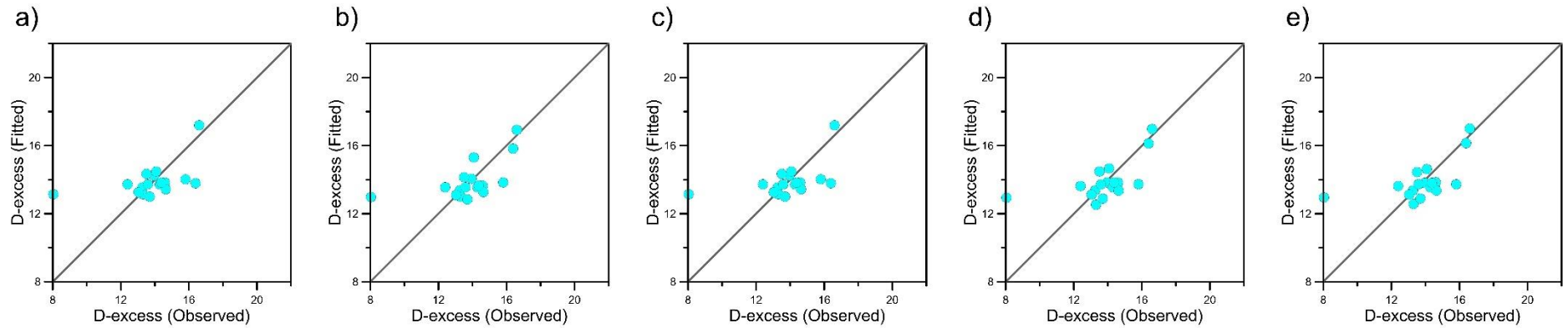


Figure A17. The x-y plot of the D-excess signal (observed against simulated) of the precipitation samples from MAM and whose trajectory crosses the Pacific coast using MLR with different number of variables. a) MLR using 1 variable, b) MLR using 2 variables, c) MLR using 3 variables, d) MLR using 4 variables and e) MLR using 5 variables.

Table A15. Results of the MRLs of the D-excess signal from the precipitation samples from MAM and whose trajectory crosses the Pacific coast using 1 until 5 variables.

Isotopic composition	Model	Variables	R ²	R ² _{aj}	AIC	RMSE	pVal	n
D-excess	M1	HR ₆	0.250	0.203	72.797	1.547	3.47E-02	18
	M2	HR ₆ , Prec ₈	0.343	0.256	72.403	1.448	4.27E-02	
	M3	HR ₆ , Prec ₈ , M+H+VH	0.360	0.223	73.945	1.429	9.16E-02	
	M4	HR ₆ , Prec ₈ , M+H+VH, Prec ₁	0.361	0.164	75.917	1.428	1.83E-01	
	M5	HR ₆ , Prec ₈ , M+H+VH, Prec ₁ , WindVeli	0.361	0.095	77.914	1.428	3.07E-01	

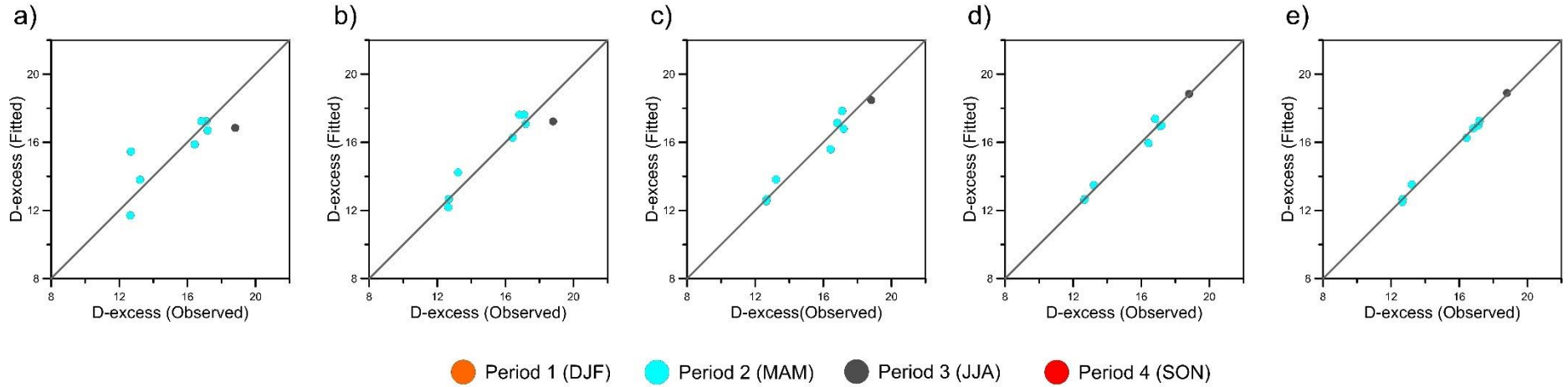


Figure A18. The x-y plot of the D-excess signal (observed against simulated) of the precipitation samples whose trajectory crosses the Mato Grosso Massif during the full study period using MLR with different number of variables. a) MLR using 1 variable, b) MLR using 2 variables, c) MLR using 3 variables, d) MLR using 4 variables and e) MLR using 5 variables.

Table A16. Results of the MRLs of the D-excess signal from the precipitation samples whose trajectory crosses the Mato Grosso Massif during the full study period using 1 until 5 variables.

Isotopic composition	Model	Variables	R ²	R ² _{aj}	AIC	RMSE	pVal	n
D-excess	M1	HR _i	0.663	0.607	32.899	3.341	1.38E-02	8
	M2	HR _i , Prec ₅	0.884	0.837	26.406	2.424	4.63E-03	
	M3	HR _i , Prec ₅ , WindVel _i	0.951	0.914	21.501	0.990	4.45E-03	
	M4	HR _i , Prec ₅ , WindVel _i , Temp _i	0.983	0.960	15.064	0.964	5.54E-03	
	M5	HR _i , Prec ₅ , WindVel _i , Temp _i , Prec ₇	0.996	0.985	5.816	0.935	1.05E-02	

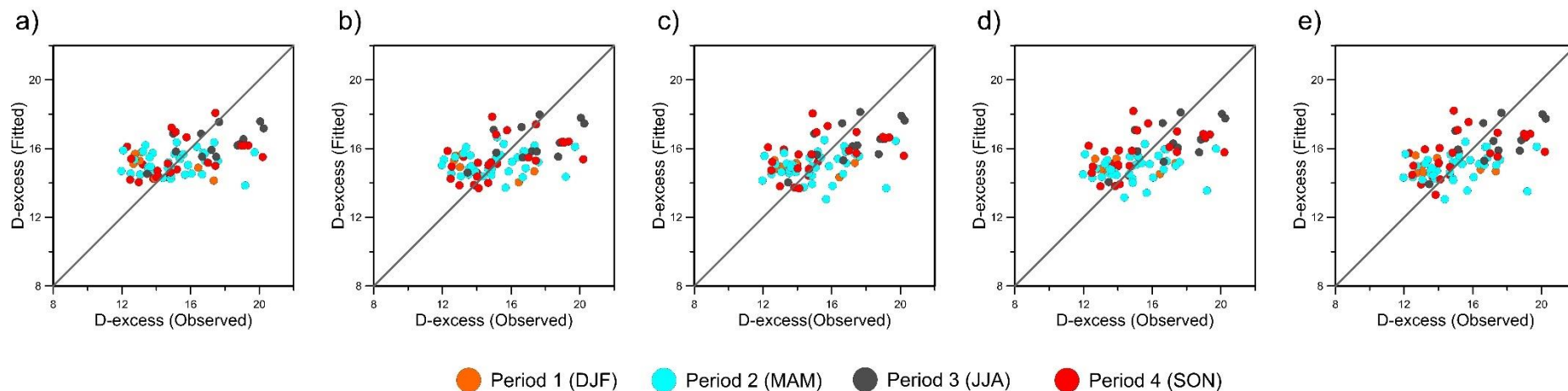


Figure A 19. The x-y plot of the D-excess signal (observed against simulated) of the precipitation samples whose trajectory crosses the Amazon basin and whose origin are between 5°N and 5°S for the full study period using MLR with different number of variables. a) MLR using 1 variable, b) MLR using 2 variables, c) MLR using 3 variables, d) MLR using 4 variables and e) MLR using 5 variables.

Table A17. Results of the MRLs of the D-excess signal from the precipitation samples whose trajectory crosses Amazon basin and whose origin are between 5°N and 5°S during the full study period using 1 until 5 variables.

Isotopic composition	Model	Variables	R ²	R ² _{aj}	AIC	RMSE	pVal	n
D-excess	M1	Temp _i	0.178	0.167	343.253	1.992	9.92E-05	80
	M2	Temp _i , Alt ₁	0.204	0.183	342.626	1.959	1.52E-04	
	M3	Temp _i , Alt ₁ , Prec ₆	0.241	0.211	340.834	1.913	1.01E-04	
	M4	Temp _i , Alt ₁ , Prec ₆ , Prec	0.252	0.213	341.614	1.899	1.91E-04	
	M5	Temp _i , Alt ₁ , Prec ₆ , Prec ₃ , RH _i	0.260	0.210	342.754	1.888	3.74E-04	

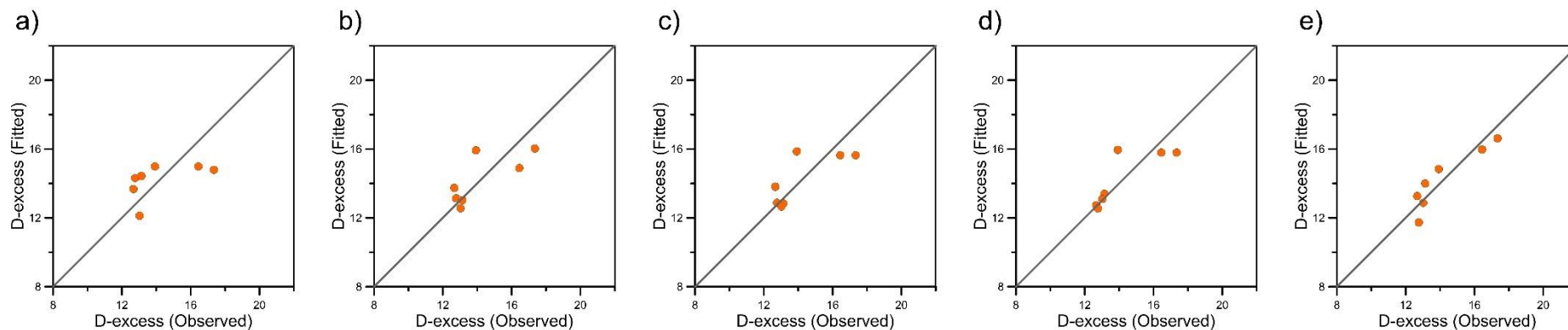


Figure A20. The x-y plot of the D-excess signal (observed against simulated) of the precipitation samples from DJF and whose trajectory crosses the Amazon basin and whose origin are between 5°N and 5°S using MLR with different number of variables. a) MLR using 1 variable, b) MLR using 2 variables, c) MLR using 3 variables, d) MLR using 4 variables and e) MLR using 5 variables.

Table A18. Results of the MRLs of the D-excess signal from the precipitation samples from DJF and whose trajectory crosses the Amazon basin and whose origin are between 5°N and 5°S using 1 until 5 variables.

Isotopic composition	Model	Variables	R ²	R ² _{aj}	AIC	RMSE	pVal	n
D-excess	M1	Prec ₅	0.284	0.140	31.529	1.499	2.18E-01	7
	M2	Prec ₅ , Temp _i	0.557	0.335	30.172	1.179	1.97E-01	
	M3	Prec ₅ , Temp _i , Prec ₆	0.595	0.189	31.543	1.127	3.80E-01	
	M4	Prec ₅ , Temp _i , Prec ₆ , SRad ₃	0.678	0.033	31.942	1.005	5.41E-01	
	M5	Prec ₅ , Temp _i , Prec ₆ , SRad ₃ , SRad ₂	0.828	0.033	29.547	0.735	6.45E-01	

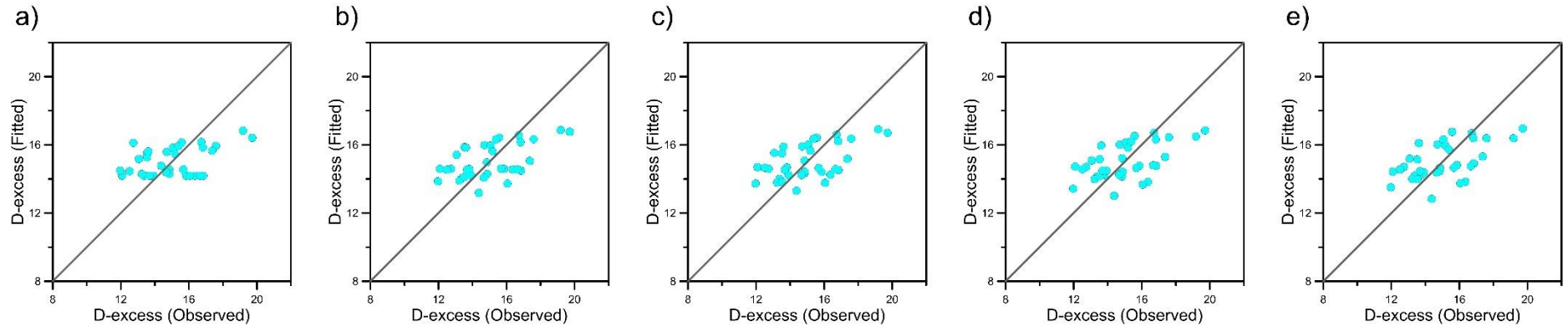


Figure A 21. The x-y plot of the D-excess signal (observed against simulated) of the precipitation samples from MAM and whose trajectory crosses the Amazon basin and whose origin are between 5°N and 5°S using MLR with different number of variables. a) MLR using 1 variable, b) MLR using 2 variables, c) MLR using 3 variables, d) MLR using 4 variables and e) MLR using 5 variables.

Table A19. Results of the MRLs of the D-excess signal from the precipitation samples from MAM and whose trajectory crosses the Amazon basin and whose origin are between 5°N and 5°S using 1 until 5 variables.

Isotopic composition	Model	Variables	R ²	R ² _{aj}	AIC	RMSE	pVal	n
D-excess	M1	M+H	0.198	0.174	140.439	1.651	7.36E-03	35
	M2	M+H, Prec ₇	0.280	0.235	138.679	1.565	5.23E-03	
	M3	M+H, Prec ₇ , PT ₄	0.285	0.215	140.451	1.560	1.45E-02	
	M4	M+H, Prec ₇ , PT ₄ , RH _i	0.299	0.206	141.725	1.544	2.65E-02	

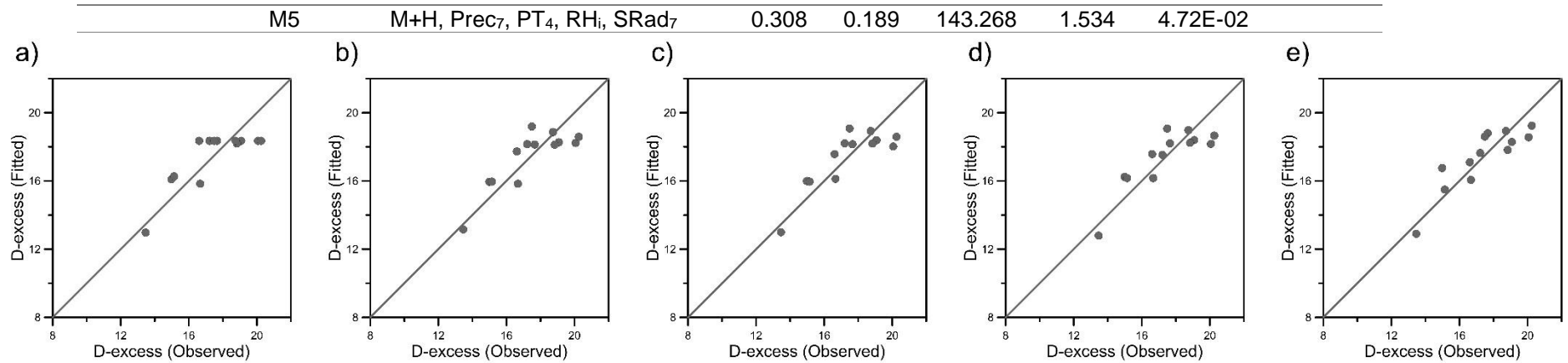


Figure A 22. The x-y plot of the D-excess signal (observed against simulated) of the precipitation samples from JJA and whose trajectory crosses the Amazon basin and whose origin are between 5°N and 5°S using MLR with different number of variables. a) MLR using 1 variable, b) MLR using 2 variables, c) MLR using 3 variables, d) MLR using 4 variables and e) MLR using 5 variables.

Table A20. Results of the MRLs of the D-excess signal from the precipitation samples from JJA and whose trajectory crosses the Amazon basin and whose origin are between 5°N and 5°S using 1 until 5 variables.

Isotopic composition	Model	Variables	R^2	R^2_{aj}	AIC	RMSE	pVal	n
D-excess	M1	Prec ₆	0.665	0.634	46.093	1.131	6.83E-04	13
	M2	Prec ₆ , SRad ₇	0.698	0.638	46.723	1.073	2.50E-03	
	M3	Prec ₆ , SRad ₇ , Press _i	0.703	0.603	48.534	1.065	9.60E-03	
	M4	Prec ₆ , SRad ₇ , Press _i , Prec ₈	0.715	0.573	49.966	1.042	2.54E-02	
	M5	Prec ₆ , SRad ₇ , Press _i , Prec ₈ , Temp _i	0.760	0.589	49.718	0.956	3.83E-02	

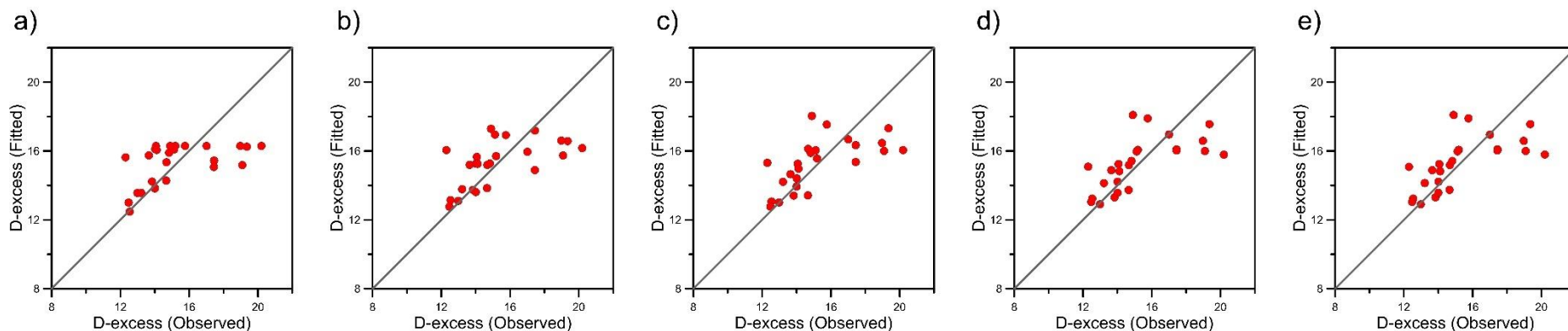


Figure A23. The x-y plot of the D-excess signal (observed against simulated) of the precipitation samples from SON and whose trajectory crosses the Amazon basin and whose origin are between 5°N and 5°S using MLR with different number of variables. a) MLR using 1 variable, b) MLR using 2 variables, c) MLR using 3 variables, d) MLR using 4 variables and e) MLR using 5 variables.

Table A21. Results of the MRLs of the D-excess signal from the precipitation samples from SON and whose trajectory crosses the Amazon basin and whose origin are between 5°N and 5°S using 1 until 5 variables.

Isotopic composition	Model	Variables	R ²	R ² _{aj}	AIC	RMSE	pVal	n
D-excess	M1	Prec ₃	0.268	0.236	109.840	1.931	8.04E-03	25
	M2	Prec ₃ , Temp _i	0.347	0.288	108.970	1.823	9.14E-03	
	M3	Prec ₃ , Temp _i , PT ₄	0.407	0.322	108.594	1.738	1.07E-02	
	M4	Prec ₃ , Temp _i , PT ₄ , RH ₈	0.428	0.314	109.662	1.706	1.97E-02	
	M5	Prec ₃ , Temp _i , PT ₄ , RH ₈ , SRad ₃	0.428	0.278	111.662	1.706	4.40E-02	

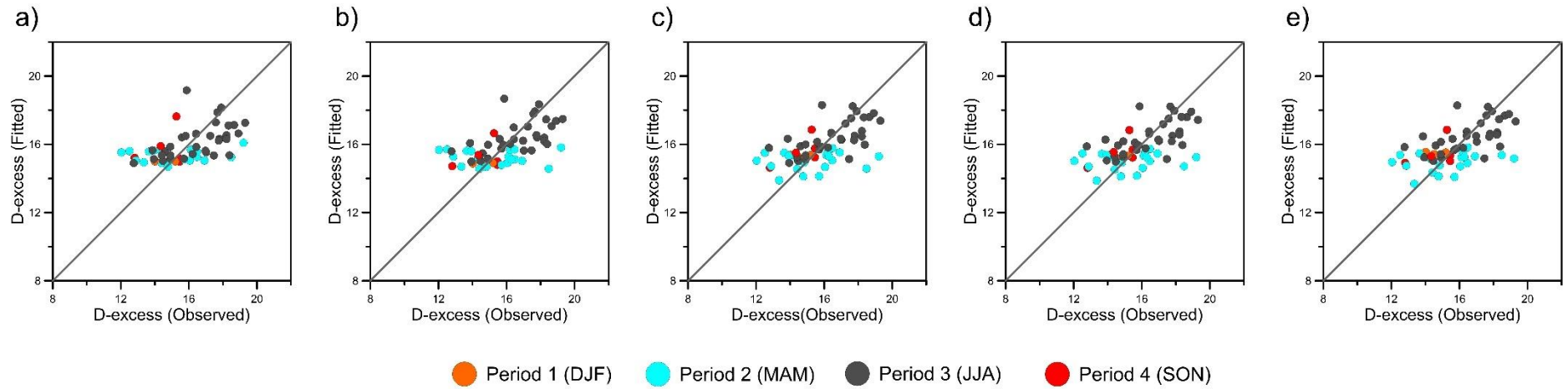


Figure A 24. The x-y plot of the D-excess signal (observed against simulated) of the precipitation samples whose trajectory crosses the Amazon basin and whose origin are under d 5°S for the full study period using MLR with different number of variables. a) MLR using 1 variable, b) MLR using 2 variables, c) MLR using 3 variables, d) MLR using 4 variables and e) MLR using 5 variables.

Table A22. Results of the MRLs of the D-excess signal from the precipitation samples whose trajectory crosses the Amazon basin and whose origin are under d 5°S during the full study period using 1 until 5 variables.

Isotopic composition	Model	Variables	R ²	R ² _{aj}	AIC	RMSE	pVal	n
D-excess	M1	HR ₆	0.254	0.242	236.717	1.555	2.91E-05	62
	M2	HR ₆ , Temp _i	0.295	0.271	235.283	1.513	3.38E-05	
	M3	HR ₆ , Temp _i , Press _i	0.330	0.295	234.091	1.474	3.30E-05	
	M4	HR ₆ , Temp _i , Press _i , Prec ₂	0.331	0.284	235.991	1.473	1.10E-04	
	M5	HR ₆ , Temp _i , Press _i , Prec ₂ , SRad ₈	0.339	0.280	237.265	1.465	2.41E-04	

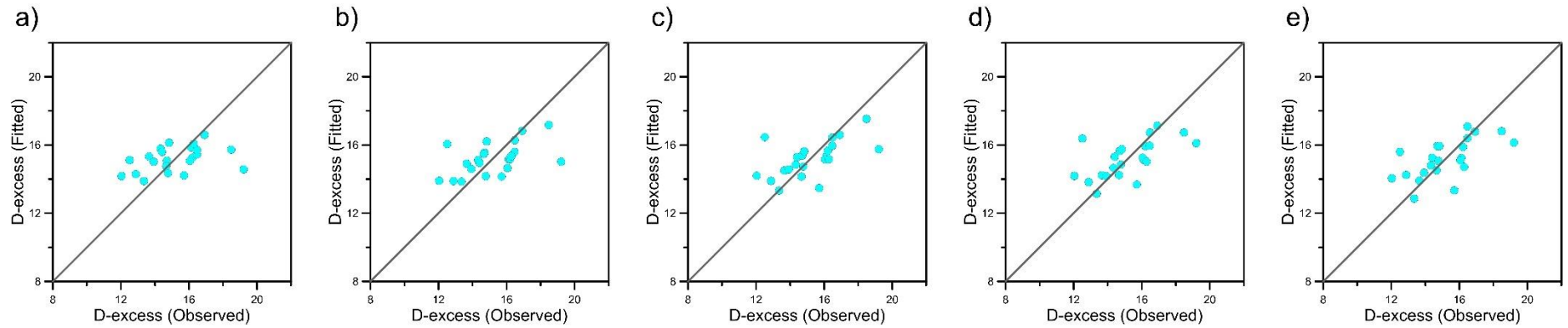


Figure A25. The x-y plot of the D-excess signal (observed against simulated) of the precipitation samples from MAM and whose trajectory crosses the Amazon basin and whose origin are under 5°S using MLR with different number of variables. a) MLR using 1 variable, b) MLR using 2 variables, c) MLR using 3 variables, d) MLR using 4 variables and e) MLR using 5 variables.

Table A23. Results of the MRLs of the D-excess signal from the precipitation samples from MAM and whose trajectory crosses the Amazon basin and whose origin are under 5°S using 1 until 5 variables.

Isotopic composition	Model	Variables	R ²	R ² _{aj}	AIC	RMSE	pVal	n
D-excess	M1	Press _i	0.159	0.117	89.884	1.628	0.066	22
	M2	Press _i , M+H	0.261	0.184	89.035	1.526	0.056	
	M3	Press _i , M+H, SRad	0.337	0.226	88.664	1.446	0.055	
	M4	Press _i , M+H, SRad _i , WindVel _i	0.362	0.212	89.803	1.418	0.089	
	M5	Press _i , M+H, SRad _i , WindVel _i , HR ₁	0.391	0.201	90.776	1.385	0.124	

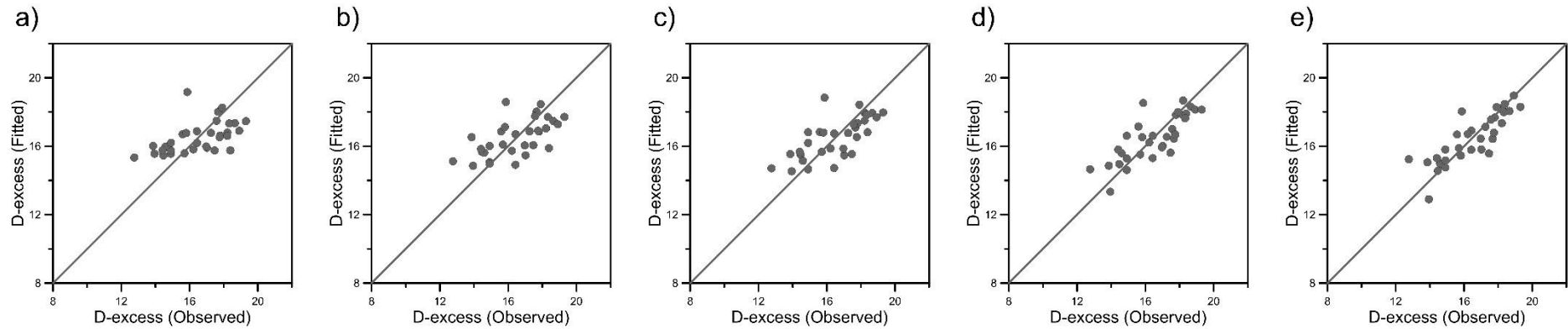


Figure A26. The x-y plot of the D-excess signal (observed against simulated) of the precipitation samples from JJA and whose trajectory crosses the Amazon basin and whose origin are under 5°S using MLR with different number of variables. a) MLR using 1 variable, b) MLR using 2 variables, c) MLR using 3 variables, d) MLR using 4 variables and e) MLR using 5 variables.

Table A 24. Results of the MRLs of the D-excess signal from the precipitation samples from JJA and whose trajectory crosses the Amazon basin and whose origin are under 5°S using 1 until 5 variables.

Isotopic composition	Model	Variables	R ²	R ² _{aj}	AIC	RMSE	pVal	n
D-excess	M1	HR ₆	0.281	0.257	119.525	1.426	1.81E-03	32
	M2	HR ₆ , Prec ₁	0.380	0.337	116.799	1.325	9.86E-04	
	M3	HR ₆ , Prec ₁ , SRad ₄	0.483	0.427	112.977	1.209	3.05E-04	
	M4	HR ₆ , Prec ₁ , SRad ₄ , Prec ₄	0.616	0.560	105.407	1.041	2.24E-05	
	M5	HR ₆ , Prec ₁ , SRad ₄ , Prec ₄ , Temp _i	0.694	0.635	100.159	0.930	5.01E-06	

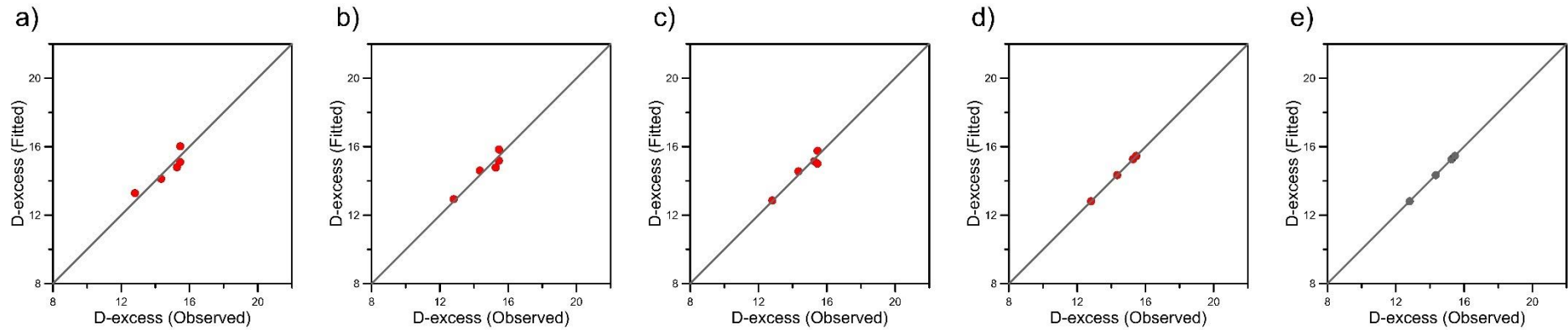


Figure A27. The x-y plot of the D-excess signal (observed against simulated) of the precipitation samples from SON and whose trajectory crosses the Amazon basin and whose origin are under 5°S using MLR with different number of variables. a) MLR using 1 variable, b) MLR using 2 variables, c) MLR using 3 variables, d) MLR using 4 variables and e) MLR using 5 variables.

Table A25. Results of the MRLs of the D-excess signal from the precipitation samples from SON and whose trajectory crosses the Amazon basin and whose origin are under 5°S using 1 until 5 variables.

Isotopic composition	Model	Variables	R ²	R ² _{aj}	AIC	RMSE	pVal	n
D-excess	M1	Press _i	0.821	0.762	11.756	0.430	0.034	5
	M2	Press _i , Prec ₂	0.897	0.793	11.019	0.327	0.103	
	M3	Press _i , Prec ₂ , SRad _i	0.932	0.729	10.903	0.265	0.328	
	M4	Press _i , Prec ₂ , SRad _i , HR ₈	1.000	-	-	-	-	
	M5	Press _i , Prec ₂ , SRad _i , HR ₈ , Press ₃	1.000	-	-	-	-	

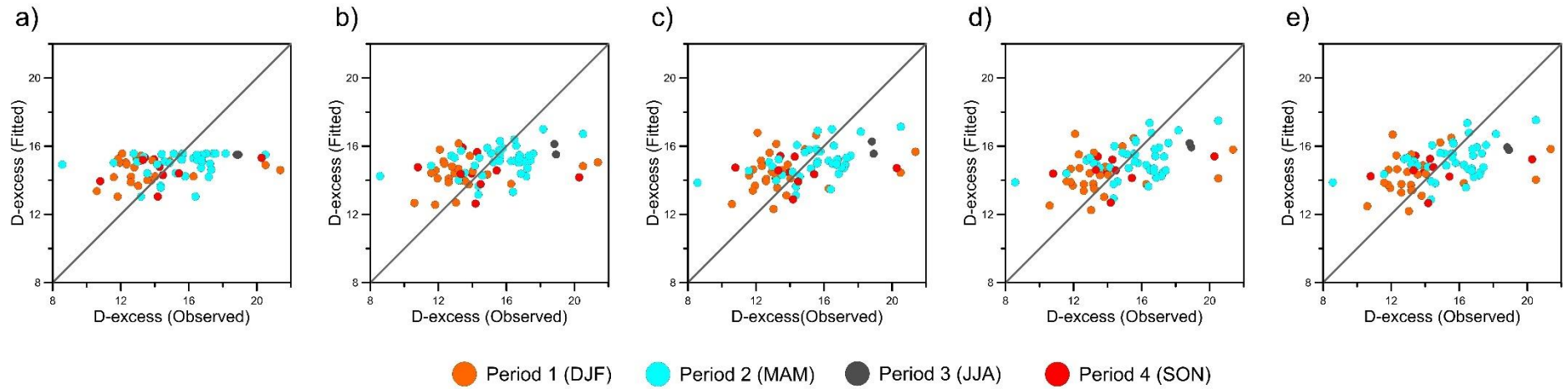


Figure A28. The x-y plot of the D-excess signal (observed against simulated) of the precipitation samples whose trajectory crosses the Amazon basin and whose origin are above 5°N for the full study period using MLR with different number of variables. a) MLR using 1 variable, b) MLR using 2 variables, c) MLR using 3 variables, d) MLR using 4 variables and e) MLR using 5 variables.

Table A26. Results of the MRLs of the D-excess signal from the precipitation samples whose trajectory crosses the Amazon basin and whose origin are above d 5°N during the full study period using 1 until 5 variables.

Isotopic composition	Model	Variables	R ²	R ² _{aj}	AIC	RMSE	pVal	n
D-excess	M1	H+VH	0.079	0.072	350.899	2.340	1.08E-02	76
	M2	H+VH, PT ₁	0.141	0.124	347.460	2.258	2.92E-03	
	M3	H+VH, PT ₁ , RH ₃	0.174	0.142	346.888	2.220	2.85E-03	
	M4	H+VH, PT ₁ , RH ₃ , Press _i	0.210	0.156	346.536	2.186	2.80E-03	
	M5	H+VH, PT ₁ , RH ₃ , Press _i , Temp _i	0.211	0.146	348.373	2.183	6.28E-03	

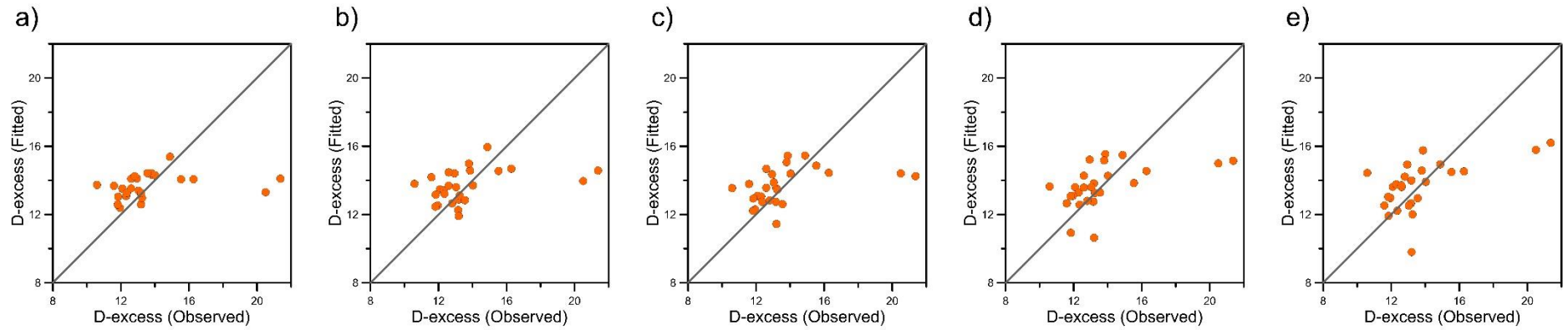


Figure A 29. The x-y plot of the D-excess signal (observed against simulated) of the precipitation samples from DJF and whose trajectory crosses the Amazon basin and whose origin are above 5°N using MLR with different number of variables. a) MLR using 1 variable, b) MLR using 2 variables, c) MLR using 3 variables, d) MLR using 4 variables and e) MLR using 5 variables.

Table A27. Results of the MRLs of the D-excess signal from the precipitation samples from DJF and whose trajectory crosses the Amazon basin and whose origin are above 5°N using 1 until 5 variables.

Isotopic composition	Model	Variables	R ²	R ² _{aj}	AIC	RMSE	pVal	n
D-excess	M1	Temp _i	0.079	0.041	123.636	2.324	0.164	26
	M2	Temp _i , SRad ₇	0.151	0.077	123.524	2.232	0.152	
	M3	Temp _i , SRad ₇ , SRad ₃	0.178	0.065	124.698	2.196	0.222	
	M4	Temp _i , SRad ₇ , SRad ₃ , Prec ₂	0.253	0.111	124.193	2.093	0.171	
	M5	Temp _i , SRad ₇ , SRad ₃ , Prec ₂ , SRad _i	0.326	0.158	123.519	1.988	0.133	

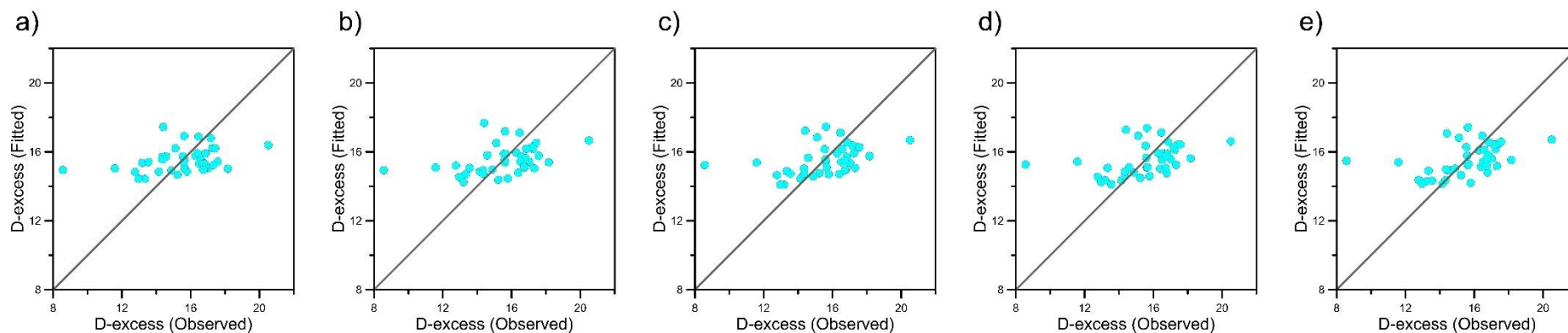


Figure A30. The x-y plot of the D-excess signal (observed against simulated) of the precipitation samples from DJF and whose trajectory crosses the Amazon basin and whose origin are above 5°N using MLR with different number of variables. a) MLR using 1 variable, b) MLR using 2 variables, c) MLR using 3 variables, d) MLR using 4 variables and e) MLR using 5 variables.

Table A28. Results of the MRLs of the D-excess signal from the precipitation samples from DJF and whose trajectory crosses the Amazon basin and whose origin are above 5°N using 1 until 5 variables.

Isotopic composition	Model	Variables	R ²	R ² _{aj}	AIC	RMSE	pVal	n
D-excess	M1	RH ₃	0.131	0.104	167.640	2.009	3.49E-02	39
	M2	RH ₃ , H+VH	0.168	0.115	167.947	1.965	5.10E-02	
	M3	RH ₃ , H+VH, SRad ₆	0.191	0.110	168.952	1.940	7.95E-02	
	M4	RH ₃ , H+VH, SRad ₆ , Prec ₄	0.191	0.080	170.398	1.936	1.27E-01	

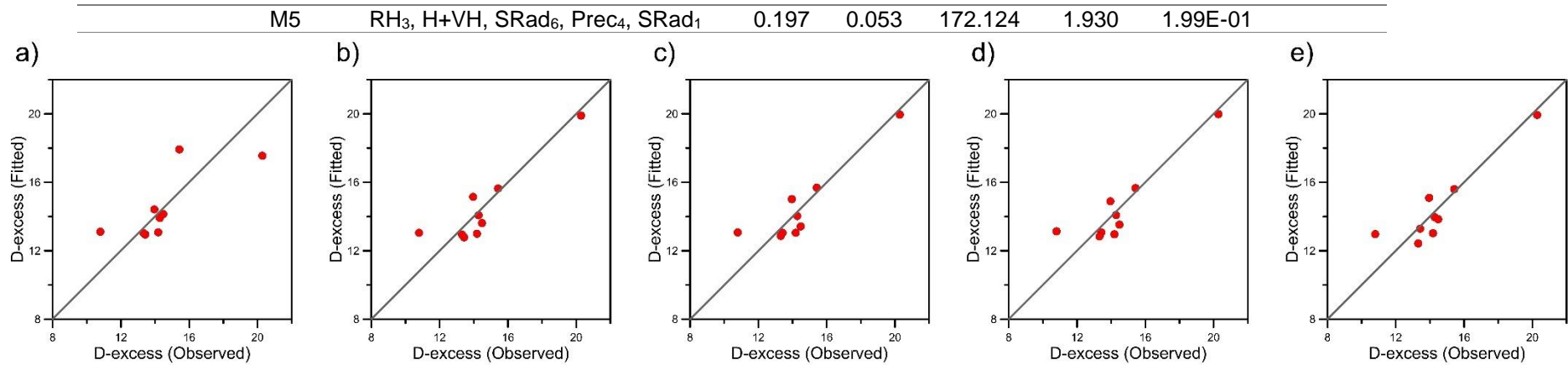


Figure A31. The x-y plot of the D-excess signal (observed against simulated) of the precipitation samples from SON and whose trajectory crosses the Amazon basin and whose origin are above 5°N using MLR with different number of variables. a) MLR using 1 variable, b) MLR using 2 variables, c) MLR using 3 variables, d) MLR using 4 variables and e) MLR using 5 variables.

Table A 29. Results of the MRLs of the D-excess signal from the precipitation samples from SON and whose trajectory crosses the Amazon basin and whose origin are above 5°N using 1 until 5 variables.

Isotopic composition	Model	Variables	R ²	R ² _{aj}	AIC	RMSE	pVal	n
D-excess	M1	Prec ₁	0.588	0.529	39.174	1.528	1.59E-02	9
	M2	Prec ₁ , Prec ₆	0.815	0.753	33.974	1.024	6.35E-03	
	M3	Prec ₁ , Prec ₆ , MD ₆	0.818	0.708	35.836	1.017	2.70E-02	
	M4	Prec ₁ , Prec ₆ , MD ₆ , SRad ₇	0.818	0.637	37.794	1.014	8.69E-02	
	M5	Prec ₁ , Prec ₆ , MD ₆ , SRad ₇ , SRad ₆	0.827	0.538	39.379	0.991	2.08E-01	

